CHAPTER 6

Inhomogeneous Fluids

Chapters 4 and 5 were concerned with theories designed primarily for the calculation of thermodynamic and structural properties of bulk, uniform fluids. We now turn our attention to non-uniform systems. The translational symmetry characteristic of a homogeneous fluid is broken by exposure to an external force field, in the vicinity of a confining surface (which may be regarded as the source of an external field), or in the presence of an interface between coexisting phases. Static properties of inhomogeneous fluids are most effectively studied within the framework of density-functional theory, the foundations of which were laid in Sections 3.1 and 3.4. As we saw there, use of the theory requires as a starting point some approximate expression for the intrinsic free energy as a functional of the single-particle density, or density profile, $\rho^{(1)}(\mathbf{r})$. In this chapter we show how useful approximations can be devised and describe their application to a variety of physical problems.

6.1 LIQUIDS AT INTERFACES

Molecular interactions at fluid interfaces are responsible for many familiar, physical processes, from lubrication and bubble formation to the wetting of solids and the capillary rise of liquids in narrow tubes. Questions of a fundamental character that a theory needs to address include the nature of the interface that arises spontaneously between, say, a liquid and its vapour or between two immiscible liquids; the layering of dense fluids near a solid substrate; the properties of liquids confined to narrow pores; the formation of electric double layers in electrolyte solutions; and the factors that control interfacial phase transitions, such as the capillary condensation of under-saturated vapour in porous media. In all these situations, surface contributions to the thermodynamic potentials (proportional to the surface area) are no longer negligible compared with the contributions from the bulk (proportional to the volume). The equilibrium values of the potentials are therefore determined by the competition between bulk and surface effects.[1]

The change in grand potential associated with an infinitesimal change in thermodynamic state of a system containing an interface is given by a generalisation of (2.4.3):

$$\mathrm{d}\Omega = -S\,\mathrm{d}T - P\,\mathrm{d}V - N\mathrm{d}\mu + \gamma\,\mathrm{d}\mathcal{A} \tag{6.1.1a}$$

or, in the case of a mixture:

$$\mathrm{d}\Omega = -S\,\mathrm{d}T - P\,\mathrm{d}V - \sum_{\nu} N_\nu\,\mathrm{d}\mu_\nu + \gamma\,\mathrm{d}\mathcal{A} \tag{6.1.1b}$$

where ν labels a species, $\mathcal{A}$ is the interfacial area and γ, the variable conjugate to $\mathcal{A}$, is the surface tension. The corresponding change in Helmholtz free energy is

$$\mathrm{d}F = -S\,\mathrm{d}T - P\,\mathrm{d}V + \sum_{\nu} \mu_\nu\,\mathrm{d}N_\nu + \gamma\,\mathrm{d}\mathcal{A} \tag{6.1.2}$$

The surface tension is the work required to increase the interface by unit area. It is positive for any real liquid, since intermolecular forces tend to reduce the interfacial area. Hence, in the absence of gravity, formation of a spherical interface is always favoured. From (6.1.1) and (6.1.2) it follows that γ may be written as a thermodynamic derivative in either of two different ways:

$$\gamma = \left(\frac{\partial\Omega}{\partial\mathcal{A}}\right)_{V,T,\{\mu_\nu\}} = \left(\frac{\partial F}{\partial\mathcal{A}}\right)_{V,T,\{N_\nu\}} \tag{6.1.3}$$

In addition, since Ω is a homogeneous function of first order in V and $\mathcal{A}$, (6.1.1) can be integrated at constant μ_ν and T to give

$$\Omega = -PV + \gamma\mathcal{A} \tag{6.1.4}$$

which is the generalisation to interfacial systems of the thermodynamic relation (2.4.2). Thus the surface tension can also be written as:

$$\gamma = \frac{1}{\mathcal{A}}(\Omega + PV) \equiv \frac{\Omega^{(\mathrm{s})}}{\mathcal{A}} \tag{6.1.5}$$

where $\Omega^{(\mathrm{s})}$ is the *surface excess* grand potential.

The concept of a surface excess property is easily extended to other thermodynamic quantities. Consider, for example, the interface between a one-component liquid and its vapour. Under the influence of gravity, the interface is planar and horizontal, and the density profile depends only on the vertical coordinate, z. Macroscopically the interface appears sharp, but on the molecular scale it varies smoothly over a few molecular diameters. A typical density profile, $\rho^{(1)}(z)$, is shown schematically in Figure 6.1, where the z-axis is drawn perpendicular to the interface. The physical interface is divided into two parts by an imaginary plane located at $z = z_0$, called the *Gibbs dividing surface*. The liquid phase extends below $z = z_0$, where $\rho^{(1)}(z)$ rapidly approaches its bulk-liquid value, ρ_{L}, while for $z > z_0$, $\rho^{(1)}(z)$ tends towards the bulk-gas value, ρ_{G}. The liquid and gas *adsorptions*, Γ_{L} and Γ_{G}, are defined as integrals over the regions labelled 1 and 2 in the figure:

$$\Gamma_{\mathrm{L}} = \int_{-\infty}^{z_0} \left[\rho^{(1)}(z) - \rho_{\mathrm{L}}\right]\mathrm{d}z < 0, \qquad \Gamma_{\mathrm{G}} = \int_{z_0}^{\infty} \left[\rho^{(1)}(z) - \rho_{\mathrm{G}}\right]\mathrm{d}z > 0 \tag{6.1.6}$$

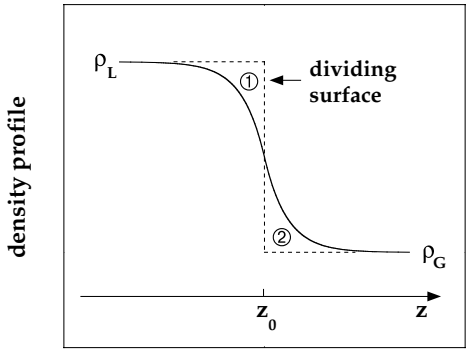

FIG. 6.1. Density profile at the liquid–vapour interface. The z-axis is perpendicular to the interface and the Gibbs dividing surface is located at $z = z_0$; ρ_L and ρ_G are the bulk densities of liquid and gas, respectively.

Though the location of the dividing surface is arbitrary, it is commonly positioned so as to make the two labelled regions equal in area, in which case the total adsorption, $\Gamma = \Gamma_L + \Gamma_G$, is zero. We shall follow this convention. If the interface were infinitely sharp, with the two bulk phases meeting discontinuously at the dividing surface, the total number of particles would be

$$N_L + N_G = V_L \rho_L + V_G \rho_G \tag{6.1.7}$$

where V_L, V_G are the volumes occupied by the two phases. The total number of particles in the inhomogeneous system contained in the volume $V = V_L + V_G$ may therefore be written as

$$N = N_L + N_G + N^{(s)} \tag{6.1.8}$$

where $N^{(s)}$ is the surface excess number of particles, and the total adsorption is $\Gamma = N^{(s)}/\mathcal{A}$. With the conventional choice of z_0, $N^{(s)} = 0$. In a solution, z_0 may be chosen such that the adsorption of the solvent vanishes, but the adsorptions of the solutes will then in general be non-zero. Expressions analogous to (6.1.8) serve as definitions of the other surface excess quantities.

The surface excess grand potential is related to the surface tension by (6.1.5). When that relation is combined with (6.1.1) and the corresponding expressions for the two bulk phases, we find that

$$\mathrm{d}\Omega^{(s)} = \gamma\,\mathrm{d}\mathcal{A} + \mathcal{A}\,\mathrm{d}\gamma = -S^{(s)}\,\mathrm{d}T - \sum_\nu N_\nu^{(s)}\,\mathrm{d}\mu_\nu + \gamma\,\mathrm{d}\mathcal{A} \tag{6.1.9}$$

which leads, after division by $\mathcal{A}$, to

$$s^{(s)}\,\mathrm{d}T + \sum_\nu \Gamma_\nu\,\mathrm{d}\mu_\nu + \mathrm{d}\gamma = 0 \tag{6.1.10}$$

where $s^{(s)} \equiv S^{(s)}/\mathcal{A}$ is the surface excess entropy per unit area. Equation (6.1.10) is called the *Gibbs adsorption equation*. This is the surface equivalent of the Gibbs–Duhem relation

in the bulk phase and shows that the adsorptions of the different species are related to the surface tension by

$$\Gamma_\nu = -\left(\frac{\partial\gamma}{\partial\mu_\nu}\right)_{T,\{\mu_{\nu'\neq\nu}\}} \tag{6.1.11}$$

Equations (6.1.10) and (6.1.11) have been derived with the example of a liquid–gas interface in mind, but their applicability is more general. They hold also in the case of a fluid in contact with a solid surface. There, depending on the nature of the solid–fluid interaction, the adsorptions may be either positive or negative.

Thus far we have assumed that the system contains a single, planar (or weakly curved) interface, well-separated from any other surface. When a fluid is narrowly confined, an additional control variable comes into play, namely the quantity that characterises the spacing between the bounding surfaces. In the simplest case, that of a liquid confined to a slit-like pore between two parallel plates of area $\mathcal{A}$, the new variable is the spacing L of the plates. The necessary generalisation of (6.1.1) is

$$\mathrm{d}\Omega = -S\,\mathrm{d}T - P\,\mathrm{d}V - \sum_\nu N_\nu\,\mathrm{d}\mu_\nu + 2\gamma\,\mathrm{d}\mathcal{A} - f_S\mathcal{A}\,\mathrm{d}L \tag{6.1.12}$$

where $\gamma = \frac{1}{2}(\partial\Omega/\partial\mathcal{A})_{V,T,\{\mu_\nu\},L}$ is the substrate–fluid interfacial tension. The quantity $-f_S$ is the variable per unit area conjugate to L; f_S has the dimensions of pressure, but is commonly referred to as the "solvation force". Physically, f_S is the force over and above any direct interaction between the plates that must be exerted on the plates in order to maintain them at a separation L; when $f_S > 0$, the force is repulsive. If Γ_ν, $\rho_\nu^{(1)}(z)$ and $\rho_{\nu\mathrm{L}}$ are, respectively, the total adsorption, density profile and bulk-liquid density of species ν, then

$$\Gamma_\nu = \int_0^L \left[\rho_\nu^{(1)}(z) - \rho_{\nu\mathrm{L}}\right]\mathrm{d}z \tag{6.1.13}$$

and the differential of the surface excess grand potential is

$$\mathrm{d}\Omega^{(\mathrm{s})} = -2s^{(\mathrm{s})}\mathcal{A}\,\mathrm{d}T - \mathcal{A}\sum_\nu \Gamma_\nu\,\mathrm{d}\mu_\nu + 2\gamma\,\mathrm{d}\mathcal{A} - f_S\mathcal{A}\,\mathrm{d}L \tag{6.1.14}$$

The interfacial tension is again the surface excess grand potential per unit area, i.e. $\gamma = \Omega^{(s)}(\mu, T, L)/2\mathcal{A}$, and the solvation force is

$$f_S = -2\left(\frac{\partial\gamma}{\partial L}\right)_{T,\{\mu_\nu\}} = -\frac{1}{\mathcal{A}}\left(\frac{\partial\Omega}{\partial L}\right)_{\mathcal{A},T,\{\mu_\nu\}} - P \tag{6.1.15}$$

since $\mathrm{d}V = \mathcal{A}\,\mathrm{d}L$. In the limit $L \to \infty$, the first term on the right-hand side of (6.1.15) becomes equal to the bulk pressure and the solvation force vanishes. In the same limit, the total adsorptions Γ_ν become equal to the sum of the adsorptions at each plate 1, 2 considered separately, i.e. $\Gamma_\nu \to \Gamma_\nu^{(1)} + \Gamma_\nu^{(2)}$, and $2\gamma \to \gamma^{(1)} + \gamma^{(2)}$. The "solvation potential"

per unit area is defined as

$$W(L) = \frac{1}{\mathcal{A}}\big[\Omega^{(\mathrm{s})}(L) - \Omega^{(\mathrm{s})}(L \to \infty)\big] = \big(2\gamma - \gamma^{(1)} - \gamma^{(2)}\big) - f_{\mathrm{S}} L \tag{6.1.16}$$

with $f_{\mathrm{S}} = -\partial W(L)/\partial L$. In the limit $L \to 0$, the confined fluid is completely expelled and $\gamma \to 0$. Thus $W(L=0) = -\gamma^{(1)} - \gamma^{(2)}$.

6.2 APPROXIMATE FREE-ENERGY FUNCTIONALS

We saw in Chapter 3 that the grand potential of an inhomogeneous fluid is a functional of the intrinsic chemical potential $\psi(\mathbf{r}) = \mu - \phi(\mathbf{r})$, where $\phi(\mathbf{r})$ is the external potential. Equation (3.3.13) shows that Ω is also the generating functional for the set of n-particle correlation functions $H^{(n)}(\mathbf{r}_1, \ldots, \mathbf{r}_n)$. Similarly, the Helmholtz free energy is a functional of the single-particle density, and its excess (non-ideal) part is the generating functional for the set of n-particle direct correlation functions $c^{(n)}(\mathbf{r}_1, \ldots, \mathbf{r}_n)$. Implementation of density-functional theory is based on the variational principle embodied in (3.4.3), according to which the functional $\Omega_\phi[n] = \mathcal{F}[n] - \int n(\mathbf{r})\psi(\mathbf{r})\,\mathrm{d}\mathbf{r}$ reaches its minimum value when the trial density $n(\mathbf{r})$ coincides with the equilibrium density, while the minimum value itself is the grand potential of the system. This in turn requires the construction of an intrinsic free-energy functional $\mathcal{F}$ in a form appropriate to the physical problem of interest. While the ideal part is given exactly by (3.1.22), the non-trivial, excess part is in general unknown, and some approximation must be invoked.

We consider first the case of a small-amplitude modulation of the single-particle density of the form $\delta\rho^{(1)}(\mathbf{r}) = \rho^{(1)}(\mathbf{r}) - \rho_0$, where ρ_0 is the number density of the uniform, reference fluid. If the modulation is produced by a weak, external potential $\delta\phi(\mathbf{r})$, the Fourier components of $\delta\rho^{(1)}$ are related to those of $\delta\phi$ by the linear-response formula (3.6.9), the constant of proportionality being the density response function $\chi(k)$. A similar result emerges if $\mathcal{F}$ is assumed to be a quadratic functional of the density modulation, i.e.

$$\mathcal{F}\big[\rho^{(1)}\big] = V f_0 + \tfrac{1}{2}\int \mathrm{d}\mathbf{r} \int \mathrm{d}\mathbf{r}'\, \delta\rho^{(1)}(\mathbf{r}) X_0(\mathbf{r}, \mathbf{r}') \delta\rho^{(1)}(\mathbf{r}') + \mathcal{O}\big(\big(\delta\rho^{(1)}\big)^3\big) \tag{6.2.1}$$

where f_0 is the free-energy per unit volume of the reference system; the function $X_0(\mathbf{r}, \mathbf{r}')$ is also a property of the reference system and therefore dependent only on the separation $\mathbf{r} - \mathbf{r}'$. The absence from (6.2.1) of a term linear in $\delta\rho^{(1)}$ is explained by the fact that when $\phi(\mathbf{r}) = 0$, $\mathcal{F}[\rho^{(1)}]$ has its minimum value for a uniform density. When written in terms of Fourier components, (6.2.1) becomes

$$\mathcal{F}\big[\rho^{(1)}\big] = V f_0 + \frac{1}{2V}\sum_{\mathbf{k}} \delta\hat{\rho}^{(1)}(\mathbf{k}) \widehat{X}_0(\mathbf{k}) \delta\hat{\rho}^{(1)}(-\mathbf{k}) + \mathcal{O}\big(\delta\rho^{(1)}\big)^3 \tag{6.2.2}$$

Then, on applying the variational formula (3.4.3), where the derivative is now taken with respect to $\delta\hat{\rho}^{(1)}(\mathbf{k})$, we find that $\delta\hat{\rho}^{(1)}(\mathbf{k})$ and $\delta\hat{\phi}(\mathbf{k})$ are linearly related in the form

$$\widehat{X}_0(\mathbf{k}) \delta\hat{\rho}^{(1)}(\mathbf{k}) = -\delta\hat{\phi}(\mathbf{k}) \tag{6.2.3}$$

Comparison of (6.2.3) with the linear-response expression (3.6.9) shows that

$$\widehat{X}_0(\mathbf{k}) \equiv -\frac{1}{\chi(k)} = \frac{k_{\mathrm{B}}T}{\rho_0 S(\mathbf{k})} \tag{6.2.4}$$

where $S(\mathbf{k})$ is the static structure factor of the uniform fluid. The free-energy cost $\delta\mathcal{F}$ of creating a weak density modulation of wavevector $\mathbf{k}$ is therefore proportional to $1/S(\mathbf{k})$.

Next we consider the slow-modulation limit, corresponding to the case of an inhomogeneity of wavelength such that $|\nabla\rho^{(1)}(\mathbf{r})|/\rho_0 = 1/\xi \ll 1/\xi_0$, where ξ_0 is a typical correlation length in the bulk system. The simplest assumption to make is that macroscopic thermodynamics applies locally, i.e. within volume elements of order ξ^3, and hence that a local free energy can be defined at each point in the fluid. In this *local-density approximation* the intrinsic free energy is written as

$$\mathcal{F}\big[\rho^{(1)}\big] = \int f\big(\rho^{(1)}\big)\,\mathrm{d}\mathbf{r} \tag{6.2.5}$$

where $f(\rho^{(1)})$ is the free-energy per unit volume of the homogeneous fluid at a density $\rho^{(1)}(\mathbf{r})$. Because the ideal contribution to the free-energy functional is precisely of the local form represented by (6.2.5), the approximation is needed only for the excess part, $\mathcal{F}^{\mathrm{ex}}$. The Euler–Lagrange formula that results from substitution of (6.2.5) in the variational formula (3.4.3) is

$$f'\big(\rho^{(1)}\big) = \mu - \phi(\mathbf{r}) \tag{6.2.6}$$

where, here and below, the prime denotes a derivative of a function with respect to its argument, in this case $\rho^{(1)}(\mathbf{r})$. If we now take the gradient of both sides of (6.2.6) and use the second of the thermodynamic relations (2.3.8), we find that (6.2.6) is equivalent to the macroscopic condition of mechanical equilibrium:

$$\nabla P(\mathbf{r}) = -\rho^{(1)}(\mathbf{r})\nabla\phi(\mathbf{r}) \tag{6.2.7}$$

The local-density approximation has proved successful in predicting the concentration profiles of colloidal dispersions in sedimentation equilibrium, where the external potential is either gravity or a centrifugal potential and the slow-modulation criterion is therefore well satisfied.[2]

To go beyond the local-density approximation we suppose initially that the inhomogeneity extends in only one direction, as is true, for example, of the interface pictured in Figure 6.1. The density profile is then a function of a single coordinate, which we take to be z. The free-energy functional can be formally expanded in powers of $1/\xi$, the inverse range of the inhomogeneity. Thus, since $\mathrm{d}\rho^{(1)}(z)/\mathrm{d}z$ is of order $1/\xi$, a natural generalisation of (6.2.5) is one in which the free-energy density f is taken to be a function not only of $\rho^{(1)}(z)$ but also of its low-order derivatives, i.e.

$$\mathcal{F}\big[\rho^{(1)}\big] = \int_{-\infty}^{\infty} f\left(\rho^{(1)}(z), \frac{\mathrm{d}\rho^{(1)}(z)}{\mathrm{d}z}, \frac{\mathrm{d}^2\rho^{(1)}(z)}{\mathrm{d}z^2}\right)\mathrm{d}z \tag{6.2.8}$$

with

$$f = f_0 + f_1 \frac{\mathrm{d}\rho^{(1)}(z)}{\mathrm{d}z} + f_{2'} \left(\frac{\mathrm{d}\rho^{(1)}(z)}{\mathrm{d}z} \right)^2 + f_{2''} \frac{\mathrm{d}^2\rho^{(1)}(z)}{\mathrm{d}z^2} + \mathcal{O}\big(1/\xi^4\big) \tag{6.2.9}$$

where the coefficients f_n on the right-hand side are all functions of $\rho^{(1)}(z)$. Terms beyond f_0 in (6.2.9) represent successive "gradient" corrections to the local-density approximation. However, the coefficient f_1 is zero, since the functional must be invariant under reflection. Indeed, if $\rho^{(1)}(z)$ is a solution of (3.4.3), the mirror-image profile $\rho^{(1)}(-z)$ must also be a solution. A change of variable from z to $z' = -z$ in the integral (6.2.8) proves that this is possible only if $f_1 = 0$; a similar argument shows that all odd coefficients must also vanish. When (6.2.9) is substituted in (6.2.8), the term involving $\mathrm{d}^2\rho^{(1)}(z)/\mathrm{d}z^2$ can be transformed into one proportional to $[\mathrm{d}\rho^{(1)}(z)/\mathrm{d}z]^2$ through an integration by parts. The resulting expression for $\mathcal{F}$ is called the *square-gradient* functional:

$$\mathcal{F}\big[\rho^{(1)}\big] = \int_{-\infty}^{\infty} \left(f_0 + f_2 \left(\frac{\mathrm{d}\rho^{(1)}(z)}{\mathrm{d}z} \right)^2 \right) \mathrm{d}z \tag{6.2.10}$$

Substitution of (6.2.10) in (3.4.3) yields a differential equation for $\rho^{(1)}(z)$ of the form

$$f_0' - f_2' \left(\frac{\mathrm{d}\rho^{(1)}(z)}{\mathrm{d}z} \right)^2 - 2 f_2 \frac{\mathrm{d}^2\rho^{(1)}(z)}{\mathrm{d}z^2} = \mu - \phi(z) \tag{6.2.11}$$

The generalisation of these results to the three-dimensional case is straightforward, requiring only the replacement of $\mathrm{d}\rho^{(1)}(z)/\mathrm{d}z$ by $\boldsymbol{\nabla}\rho^{(1)}(\mathbf{r})$. Thus (6.2.10) becomes

$$\mathcal{F}\big[\rho^{(1)}\big] = \int \big(f_0 + f_2 \big| \boldsymbol{\nabla}\rho^{(1)}(\mathbf{r}) \big|^2 \big) \, \mathrm{d}\mathbf{r} \tag{6.2.12}$$

where f_0 and f_2 are functions of $\rho^{(1)}(\mathbf{r})$.

The coefficient f_2 can be determined by considering again the case of a slowly varying, small-amplitude inhomogeneity $\delta\rho^{(1)}(\mathbf{r})$ around a bulk density ρ_0. If the integrand in (6.2.12) is expanded to second order in $\delta\rho^{(1)}(\mathbf{r})$ and the result expressed in terms of Fourier components, we find that

$$\begin{aligned} \mathcal{F}\big[\rho^{(1)}\big] &\approx \int \big(f_0 + \tfrac{1}{2} f_0'' \big(\delta\rho^{(1)}\big)^2 + f_2 \boldsymbol{\nabla}\delta\rho^{(1)}(\mathbf{r}) \cdot \boldsymbol{\nabla}\delta\rho^{(1)}(\mathbf{r}) \big) \, \mathrm{d}\mathbf{r} \\ &= V f_0 + \frac{1}{2V} \sum_{\mathbf{k}} \big(f_0'' + 2 f_2 k^2 \big) \delta\hat{\rho}^{(1)}(\mathbf{k}) \delta\hat{\rho}^{(1)}(-\mathbf{k}) \end{aligned} \tag{6.2.13}$$

where f_0 and f_2 are now functions of ρ_0. This result should be compared with the quadratic functional (6.2.2). Both approximations assume that the inhomogeneity is small in amplitude, but whereas (6.2.2) is valid for any $\mathbf{k}$, (6.2.13) holds only in the long-wavelength limit. The structure factor and two-particle direct correlation function of the reference fluid

are related by (3.6.10). If $\hat{c}(\mathbf{k})$ is expanded in even powers of k in the manner of (5.6.15), the quantity $\widehat{X}_0(\mathbf{k})$ in (6.2.2) can be replaced by

$$\widehat{X}_0(\mathbf{k}) = \frac{k_B T}{\rho_0}\big(1 - \rho_0 \hat{c}(k)\big) = \frac{k_B T}{\rho_0}\big(1 - c_0 - c_2 k^2 + \mathcal{O}\big(k^4\big)\big) \tag{6.2.14}$$

where the coefficients c_0 and c_2 are given by (5.6.16). Then, on identifying the resulting expression with (6.2.13), we find that

$$f_0''(\rho_0) = k_B T \int c(r)\, \mathrm{d}\mathbf{r} \tag{6.2.15a}$$

$$f_2(\rho_0) = \tfrac{1}{12} k_B T \int c(r) r^2\, \mathrm{d}\mathbf{r} \tag{6.2.15b}$$

Equation (6.2.15a) is merely a restatement of the compressibility relation (3.5.15), while (6.2.15b) shows that the coefficient f_2 is determined by the second moment of the direct correlation function of the homogeneous system.

The form of the results obtained for f_0 and f_2 suggests that terms of order higher than quadratic are likely to involve still higher-order moments of $c(r)$, thereby exposing a limitation inherent in an expansion in powers of the density-profile gradient (or powers of $1/\xi$). Because $c(r)$ decays as $v(r)$ at large r, moments of any given order will diverge for sufficiently long ranged potentials. For example, if the potential contains a contribution from dispersion forces, $c(r)$ will decay as r^{-6}, leading to a divergence of the fourth and higher-order moments and hence of the coefficients f_n for $n \geqslant 4$. Even within the square-gradient approximation there is the further difficulty that in the presence of attractive interactions the equilibrium state of the reference system may be one in which liquid and vapour coexist, and neither f_0 nor f_2 is properly defined in the two-phase region. The square-gradient functional has nonetheless proved extremely useful in studies of the liquid–gas interface, as the work described in the next section will illustrate.[3] Long-range interactions can be treated by dividing the pair potential into a short-range reference part and long-range perturbation in the spirit of the perturbation theories of Chapter 5. This separation leads to the formally exact expression for the excess part of the free-energy functional given by (3.4.10), from which an approximate, mean-field functional is obtained if the correlation term is ignored. The mean-field approach provides the basis for the Poisson–Boltzmann theory of the electric double layer described in Chapter 10.

The local-density and square-gradient functionals are both designed for use in cases where the inhomogeneity is both weak and slowly varying. Two different strategies have been devised to deal with situations in which these conditions are not met. The first, already discussed in a different context in Section 4.3, is based on a functional Taylor expansion of $\mathcal{F}^{\mathrm{ex}}$ in powers of the deviation from the bulk density. Truncation of the expansion at second order, and replacement of the direct correlation function by that of the reference system, leads to the expression for the density profile given by (4.3.16); the quadratic functional (6.2.1) is then recovered if the ideal contribution to the free energy is also expanded to second order. Equation (4.3.16) provides the starting point for a theory of freezing described in Section 6.6. The alternative approach involves the concept of a weighted or

coarse-grained local density. There are some circumstances in which the local density can reach values greater than that corresponding to close packing. This is true, for example, of a dense hard-sphere fluid close to a solid surface. In such cases the local-density approximation becomes meaningless. However, a non-local approximation with a structure not unlike (6.2.5) can be devised by introducing a coarse-grained density $\bar{\rho}(\mathbf{r})$, defined as a weighted average of $\rho^{(1)}(\mathbf{r})$ over a volume comparable with the volume of a particle, i.e.

$$\bar{\rho}(\mathbf{r}) = \int w\big(|\mathbf{r}-\mathbf{r}'|\big)\rho^{(1)}(\mathbf{r}')\,\mathrm{d}\mathbf{r}' \tag{6.2.16}$$

where $w(|\mathbf{r}|)$ is some suitable weight function, normalised such that

$$\int w\big(|\mathbf{r}|\big)\,\mathrm{d}\mathbf{r} = 1 \tag{6.2.17}$$

The excess part of the free-energy functional is then taken to be

$$\mathcal{F}^{\mathrm{ex}}\big[\rho^{(1)}\big] = \int \phi^{\mathrm{ex}}(\bar{\rho})\rho^{(1)}(\mathbf{r})\,\mathrm{d}\mathbf{r} \tag{6.2.18}$$

where $\phi^{\mathrm{ex}}(\bar{\rho}) = f^{\mathrm{ex}}(\bar{\rho})/\bar{\rho}$ is the excess free energy per particle of the homogeneous fluid at a density $\bar{\rho}(\mathbf{r})$; the exact form (3.1.22) is retained for the ideal part. Equation (6.2.18) represents a *weighted-density approximation*.

The difficulty in implementing a weighted-density approximation lies in making an appropriate choice of weight function.[4] A useful guide is obtained by considering the low-density limit. The virial expansion developed in Section 3.9 shows that to lowest order in density the excess free energy per particle of a homogeneous fluid of density ρ_0 is $\phi^{\mathrm{ex}}(\rho_0) = k_{\mathrm{B}}T\rho_0 B_2$, where B_2 is the second virial coefficient (3.9.7). In the case of hard spheres, B_2 is given by the integral

$$B_2 = \tfrac{1}{2}\int \Theta\big(|\mathbf{r}|-d\big)\,\mathrm{d}\mathbf{r} \tag{6.2.19}$$

where d is the hard-sphere diameter and $\Theta(x)$ is a unit step function: $\Theta(x) = 1$, $x < 0$; $\Theta(x) = 0$, $x > 0$. The total excess free energy of the homogeneous fluid can therefore be written as

$$\beta F^{\mathrm{ex}} = \beta\int \rho_0\phi^{\mathrm{ex}}(\rho_0)\,\mathrm{d}\mathbf{r} = \tfrac{1}{2}\int \mathrm{d}\mathbf{r}\int \mathrm{d}\mathbf{r}'\,\rho_0^2\Theta\big(|\mathbf{r}-\mathbf{r}'|-d\big) \tag{6.2.20}$$

This result is immediately generalisable to the inhomogeneous case in the form

$$\begin{aligned}\beta\mathcal{F}^{\mathrm{ex}}\big[\rho^{(1)}\big] &= \tfrac{1}{2}\int \mathrm{d}\mathbf{r}\int \mathrm{d}\mathbf{r}'\,\rho^{(1)}(\mathbf{r})\Theta\big(|\mathbf{r}-\mathbf{r}'|-d\big)\rho^{(1)}(\mathbf{r}') \\ &= \tfrac{1}{2}\beta\int \phi^{\mathrm{ex}}(\bar{\rho})\rho^{(1)}(\mathbf{r})\,\mathrm{d}\mathbf{r}\end{aligned} \tag{6.2.21}$$

where $\bar{\rho}(\mathbf{r})$ is the weighted density defined by (6.2.16), with a weight function given by

$$w\big(|\mathbf{r}|\big) = \frac{1}{2B_2}\Theta\big(|\mathbf{r}| - d\big) = \frac{3}{4\pi d^3}\Theta\big(|\mathbf{r}| - d\big) \tag{6.2.22}$$

which corresponds to averaging the density uniformly over a sphere of radius d. The same approximation may be used at higher densities if combined with a suitable expression for $\phi^{\mathrm{ex}}(\bar{\rho})$, such as that derived from the Carnahan–Starling equation of state. This leads to qualitatively satisfactory results for the oscillatory density profiles of hard spheres near hard, planar walls;[5] an example is shown later in Figure 6.4, from which the quantitative deficiencies in the approximation are evident. Significant improvement is achievable, at the cost of greater computational effort, if the weight function itself is made dependent on the weighted density.[6] For example, we can retain (6.2.18) but replace (6.2.16) by

$$\bar{\rho}(\mathbf{r}) = \int w\big(|\mathbf{r} - \mathbf{r}'|, \bar{\rho}\big)\rho^{(1)}(\mathbf{r}')\,\mathrm{d}\mathbf{r}' \tag{6.2.23}$$

Alternatively, we can write the free-energy functional in the form

$$\mathcal{F}^{\mathrm{ex}}\big[\rho^{(1)}\big] = N\phi^{\mathrm{ex}}(\bar{\rho}) \tag{6.2.24}$$

where $\bar{\rho}$ is a position-independent, weighted density given by

$$\bar{\rho} = \frac{1}{N}\int \mathrm{d}\mathbf{r}\,\rho^{(1)}(\mathbf{r}) \int \mathrm{d}\mathbf{r}'\, w\big(|\mathbf{r} - \mathbf{r}'|, \bar{\rho}\big)\rho^{(1)}(\mathbf{r}') \tag{6.2.25}$$

In either case, a solution for $w(|\mathbf{r}|, \bar{\rho})$ can be obtained by functionally differentiating $\mathcal{F}^{\mathrm{ex}}$ twice with respect to $\rho^{(1)}$ to give $c(\mathbf{r})$ (see (3.5.2)) and matching the results to those for the reference system. Numerical calculations therefore require as input not only the free energy of the uniform fluid but also the direct correlation function, which would normally be obtained from some approximate integral equation. For many purposes, however, these methods has been superseded by the *fundamental-measure theory* of Rosenfeld,[7] a discussion of which we defer until Section 6.4.

6.3 THE LIQUID–VAPOUR INTERFACE

An interface between bulk phases will form spontaneously whenever the thermodynamic conditions necessary for phase coexistence are met. The most familiar example is the interface that forms between a liquid and its coexisting vapour, for which the density profile $\rho^{(1)}(z)$ varies smoothly with the single coordinate z in the manner illustrated schematically in Figure 6.1. At low temperatures the width of the interface is of the order of a few particle diameters, but since the distinction between the two phases vanishes continuously at the critical temperature, the width is expected to increase rapidly as the critical point is approached and the densities ρ_{L} and ρ_{G} merge towards a common value, the critical density ρ_{c}. The smoothness of the profile makes this a problem to which the square-gradient

approximation is well suited. Such a calculation was first carried out by van der Waals, whose work is the earliest known example of the use in statistical mechanics of what are now called density-functional methods. The Euler–Lagrange equation to be solved is (6.2.11) in the limit in which the gravitational potential $\phi(z) = mgz$ becomes vanishingly small. So long as the inhomogeneity is of small amplitude, i.e. $(\rho_L - \rho_G) \ll \rho_c$, the coefficient f_2 of the square-gradient term is related by (6.2.15b) to the direct correlation function of the bulk, reference system. For condensation to occur, the interparticle potential must contain an attractive term, $w(r)$ say. Within the random-phase approximation, $c(r) \approx c_0(r) - \beta w(r)$ (see (3.5.17)), but the presence of a factor r^4 in the integrand means that the contribution to the integral in (6.2.15b) from the short-range function $c_0(r)$ can be ignored. Thus

$$f_2 \approx -\tfrac{1}{3}\pi \int_0^\infty w(r) r^4 \, \mathrm{d}r = \tfrac{1}{2}m \tag{6.3.1}$$

where m is a positive, density-independent constant. Equation (6.2.11) then takes the simpler form

$$m \frac{\mathrm{d}^2 \rho^{(1)}(z)}{\mathrm{d}z^2} = -\frac{\mathrm{d}W(\rho^{(1)})}{\mathrm{d}\rho^{(1)}} \tag{6.3.2}$$

where $W(\rho^{(1)}) = -f_0(\rho^{(1)}) + \mu\rho^{(1)}$. The analogy between this expression and Newton's equation of motion is obvious, with m, z, $\rho^{(1)}(z)$ and $W(\rho^{(1)})$ playing the roles of mass, time, position and potential energy, respectively. Equation (6.3.2) is a non-linear differential equation that must be solved subject to the boundary conditions $\lim_{z\to\pm\infty} W(\rho^{(1)}) = W(\rho_B) = -f_0(\rho_B) + \mu\rho_B = P$, where ρ_B is the bulk density of either liquid (as $z \to -\infty$) or gas (as $z \to +\infty$) and P is the bulk pressure. When integrated, (6.3.2) becomes

$$W\big(\rho^{(1)}\big) + \tfrac{1}{2}m\left(\frac{\mathrm{d}\rho^{(1)}(z)}{\mathrm{d}z}\right)^2 = P \tag{6.3.3}$$

which is the analogue of the conservation of mechanical energy, while a second integration yields a parametric representation of the density profile in the form of a quadrature:

$$z = -\left(\frac{m}{2}\right)^{1/2} \int_{\rho^{(1)}(0)}^{\rho^{(1)}(z)} \big[P - W(\rho)\big]^{-1/2} \, \mathrm{d}\rho \tag{6.3.4}$$

By definition, $W(\rho) = -\omega(\rho)$, where $\omega = \Omega/V$ is the grand potential per unit volume of the fluid at a density $\rho = \rho^{(1)}(z)$. At liquid–gas coexistence, $\omega(\rho)$ has two minima of equal depth, situated at $\rho = \rho_L$ and $\rho = \rho_G$, with $\omega(\rho_L) = \omega(\rho_G) = -P$. A simple parametrisation of $\omega(\rho)$, valid near the critical point is

$$\omega(\rho) = \tfrac{1}{2}C(\rho - \rho_L)^2(\rho - \rho_G)^2 - P \tag{6.3.5}$$

where both C and the pressure at coexistence, P, are functions of temperature. Substitution of (6.3.5) in (6.3.4) gives

$$z = -\left(\frac{m}{C}\right)^{1/2} \int_{\rho^{(1)}(0)}^{\rho^{(1)}(z)} \frac{\mathrm{d}\rho}{(\rho_{\mathrm{L}} - \rho)(\rho - \rho_{\mathrm{G}})} = -\zeta \ln\left(\frac{\rho^{(1)}(z) - \rho_{\mathrm{G}}}{\rho_{\mathrm{L}} - \rho^{(1)}(z)}\right) \tag{6.3.6}$$

where $\zeta = (m/C)^{1/2}/(\rho_{\mathrm{L}} - \rho_{\mathrm{G}})$ is a characteristic length that provides a measure of the interfacial width. Equation (6.3.6) is easily solved to give $\rho^{(1)}$ as a function of z:

$$\begin{aligned} \rho^{(1)}(z) &= \frac{\rho_{\mathrm{G}}}{1 + \exp(-z/\zeta)} + \frac{\rho_{\mathrm{L}}}{1 + \exp(z/\zeta)} \\ &= \tfrac{1}{2}(\rho_{\mathrm{L}} + \rho_{\mathrm{G}}) - \tfrac{1}{2}(\rho_{\mathrm{L}} - \rho_{\mathrm{G}}) \tanh\left(\frac{z}{2\zeta}\right) \end{aligned} \tag{6.3.7}$$

which has the general shape pictured in Figure 6.1. The predicted profile is therefore antisymmetric with respect to the mid-point, a result consequent on the symmetric form assumed for the grand potential in (6.3.5) and the neglect of the density dependence of the coefficient f_2. In reality, the profile is steeper on the liquid than on the vapour side. Equation (6.3.7) also implies that the width of the interface diverges at the critical point. Within the mean-field theory of phase transitions, $(\rho_{\mathrm{L}} - \rho_{\mathrm{G}})$ behaves as $(T_{\mathrm{c}} - T)^{1/2}$ as the critical temperature is approached from below,[8] so ζ diverges as $(T_{\mathrm{c}} - T)^{-1/2}$. Note, however, that density-functional theory provides only an "intrinsic" or averaged description of the density profile. The physical interface is a fluctuating object; these "capillary" fluctuations lead to a thermal broadening of the interface that can be comparable with the theoretical, intrinsic thickness.

The surface tension is defined thermodynamically as the additional free energy per unit area due to the presence of an interface. Accordingly, within the square-gradient approximation:

$$\gamma = \int_{-\infty}^{\infty} \left(f_0\big(\rho^{(1)}\big) + \tfrac{1}{2}m\big(\mathrm{d}\rho^{(1)}/\mathrm{d}z\big)^2 - f_{\mathrm{B}}\right) \mathrm{d}z \tag{6.3.8}$$

where f_{B} is the bulk free-energy density, equal to f_{L} for $z < z_0$ and to f_{G} for $z > z_0$. Now $f_0(\rho) = -W(\rho) + \mu\rho$ and $W(\rho)$ is given by (6.3.3), from which the bulk pressure can be eliminated by use of the thermodynamic relation $P = f_{\mathrm{B}} - \mu\rho_{\mathrm{B}}$. Equation (6.3.8) therefore reduces to

$$\begin{aligned} \gamma &= \int_{-\infty}^{\infty} \left(-P + \mu\rho^{(1)}(z) + m\big(\mathrm{d}\rho^{(1)}/\mathrm{d}z\big)^2 - f_B\right) \mathrm{d}z \\ &= \int_{-\infty}^{\infty} \left(\mu\big[\rho^{(1)}(z) - \rho_{\mathrm{B}}\big] + m\big(\mathrm{d}\rho^{(1)}/\mathrm{d}z\big)^2\right) \mathrm{d}z = m \int_{-\infty}^{\infty} \big(\mathrm{d}\rho^{(1)}/\mathrm{d}z\big)^2 \, \mathrm{d}z \end{aligned} \tag{6.3.9}$$

Use of (6.3.3) and (6.3.5) allows (6.3.9) to be recast in the equivalent form:

$$\gamma = m \int_{-\infty}^{\infty} \frac{\mathrm{d}\rho^{(1)}}{\mathrm{d}z} \, \mathrm{d}\rho^{(1)} = (2m)^{1/2} \int_{\rho_{\mathrm{L}}}^{\rho_{\mathrm{G}}} \big[P + \omega(\rho)\big]^{1/2} \, \mathrm{d}\rho$$

$$= -(mC)^{1/2} \int_{\rho_L}^{\rho_G} (\rho_L - \rho)(\rho - \rho_G)\, d\rho = \tfrac{1}{6}(mC)^{1/2}(\rho_L - \rho_G)^3 \qquad (6.3.10)$$

Thus, close to the critical point, the surface tension is predicted to behave as $\gamma \sim (T_c - T)^{3/2}$. Experimentally the critical exponent is found to be somewhat smaller than $\frac{3}{2}$.

6.4 FUNDAMENTAL-MEASURE THEORY

Fundamental-measure theory is a generalised form of weighted-density approximation for fluids consisting of hard particles. In contrast to similar approximations discussed in Section 6.2, the free-energy density is taken to be a function not just of one but of several different weighted densities, defined by weight functions that emphasise the geometrical characteristics of the particles. The theory was originally formulated for hard-sphere mixtures, but for the sake of simplicity we consider in detail only the one-component case. Its development[7] was inspired by the link that exists between scaled-particle theory[9] – described in Appendix E – and the Percus–Yevick approximation for hard spheres. Scaled-particle theory provides only thermodynamic properties, while the PY approximation is a theory of pair structure, but the PY equation of state obtained via the compressibility route is identical to the scaled-particle result; the same is true for binary mixtures.

The derivation of the theory starts from the observation that the PY expression (4.4.10) for the two-particle direct correlation function of the hard-sphere fluid can be rewritten in terms of quantities that characterise the geometry of two intersecting spheres of radius R ($= \frac{1}{2}d$) and separated by a distance $r < 2R$, as pictured in Figure 6.2. The quantities involved are the overlap volume $\Delta V(r)$, the overlap surface area $\Delta S(r)$ and the "overlap radius" $\Delta R(r) = 2R - \overline{R}$, where $\overline{R} = R + r/4$ is the mean radius of the convex envelope

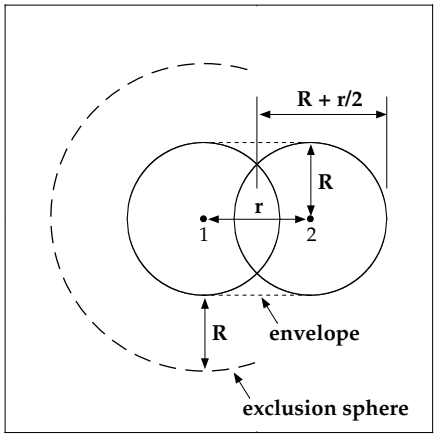

FIG. 6.2. Geometry of two overlapping hard spheres of radius R and separation r. The exclusion sphere of radius $2R$ drawn around sphere 1 defines the region into which the centre of another sphere cannot enter without creating an overlap.

surrounding the spheres. Written in this way, (4.4.10) becomes

$$-c(r) = \chi^{(3)}\Delta V(r) + \chi^{(2)}\Delta S(r) + \chi^{(1)}\Delta R(r) + \chi^{(0)}\Theta\big(|\mathbf{r}| - 2R\big) \tag{6.4.1}$$

where the step function $\Theta(|\mathbf{r}| - 2R)$, defined in the previous section, is the "characteristic" volume function of the exclusion sphere shown in the figure. The density-dependent coefficients $\chi^{(\alpha)}$ can be expressed in the form

$$\begin{aligned}
\chi^{(0)} &= \frac{1}{1-\xi_3}, \qquad \chi^{(1)} = \frac{\xi_2}{(1-\xi_3)^2} \\
\chi^{(2)} &= \frac{\xi_1}{(1-\xi_3)^2} + \frac{\xi_2^2}{4\pi(1-\xi_3)^3} \\
\chi^{(3)} &= \frac{\xi_0}{(1-\xi_3)^2} + \frac{2\xi_1\xi_2}{(1-\xi_3)^3} + \frac{\xi_2^3}{4\pi(1-\xi_3)^4}
\end{aligned} \tag{6.4.2}$$

with $\xi_\alpha = \rho\mathcal{R}^{(\alpha)}$, where the quantities $\mathcal{R}^{(\alpha)}$ are the "fundamental geometric measures" of a sphere:

$$\begin{aligned}
&\mathcal{R}^{(3)} = \tfrac{4}{3}\pi R^3 \quad \text{(volume)}, && \mathcal{R}^{(2)} = 4\pi R^2 \quad \text{(surface area)} \\
&\mathcal{R}^{(1)} = R \quad \text{(radius)}, && \mathcal{R}^{(0)} = 1
\end{aligned} \tag{6.4.3}$$

The variables ξ_α also arise naturally in scaled-particle theory. In particular, the scaled-particle free-energy density (see Appendix E) can be written as

$$\frac{\beta F^{\text{ex}}}{V} = -\xi_0\ln(1-\xi_3) + \frac{\xi_1\xi_2}{1-\xi_3} + \frac{\xi_2^3}{24\pi(1-\xi_3)^2} \tag{6.4.4}$$

The same result applies to mixtures if the scaled-particle variables are replaced by their multi-component generalisations, i.e. $\xi_\alpha = \sum_\nu \rho_\nu \mathcal{R}_\nu^{(\alpha)}$, where ρ_ν is the number density of spheres of radius R_ν and fundamental measures $\mathcal{R}_\nu^{(\alpha)}$.

The overlap volume, surface and radius are geometric measures associated with a pair of overlapping spheres, but they are also expressible in terms of convolutions of the characteristic volume and surface functions of individual spheres:

$$\omega^{(3)}(\mathbf{r}) = \Theta\big(|\mathbf{r}| - R\big) \quad \text{(volume)}, \qquad \omega^{(2)}(\mathbf{r}) = \delta\big(|\mathbf{r}| - R\big) \quad \text{(surface)} \tag{6.4.5}$$

via the relations

$$\begin{aligned}
\Delta V(r) = \omega^{(3)} \otimes \omega^{(3)} &= \int \Theta\big(|\mathbf{r}'| - R\big)\Theta\big(|\mathbf{r} - \mathbf{r}'| - R\big)\,\mathrm{d}\mathbf{r}' \\
&= \tfrac{2}{3}\pi\big(2R^3 - 3R^2 r + r^3\big)\Theta\big(|\mathbf{r}| - 2R\big) \\
\Delta S(r) = 2\omega^{(3)} \otimes \omega^{(2)} &= 2\int \Theta\big(|\mathbf{r}'| - R\big)\delta\big(|\mathbf{r} - \mathbf{r}'| - R\big)\,\mathrm{d}\mathbf{r}' \\
&= 4\pi R^2(1 - r/2R)\Theta\big(|\mathbf{r}| - 2R\big)
\end{aligned}$$

$$\Delta R(r) = \frac{\Delta S(r)}{8\pi R} + \tfrac{1}{2} R\Theta\big(|\mathbf{r}| - 2R\big) = (R - r/4)\Theta\big(|\mathbf{r}| - 2R\big) \tag{6.4.6}$$

When results are brought together, it is straightforward to show that (6.4.1) is identical to (4.4.10); in particular, $c(r)$ is strictly zero for $r > 2R$ and $c(r) \to -\Theta(|\mathbf{r}| - 2R)$ as $\rho \to 0$. It is, in addition, clear that if $c(r)$ is to be written solely in terms of functions characteristic of individual spheres, the pair function $\Theta(|\mathbf{r}| - 2R)$ must be replaced by some convolution of single-sphere functions; this can be achieved with a basis set consisting of the two scalar functions (6.4.5), a vector function

$$\boldsymbol{\omega}^{(2)}(\mathbf{r}) = \nabla\omega^{(3)}(\mathbf{r}) = \frac{\mathbf{r}}{r}\delta\big(|\mathbf{r}| - R\big) \tag{6.4.7}$$

and three further functions proportional to either $\omega^{(2)}(\mathbf{r})$ or $\boldsymbol{\omega}^{(2)}(\mathbf{r})$:

$$\omega^{(1)}(\mathbf{r}) = \frac{\omega^{(2)}(\mathbf{r})}{4\pi R}, \qquad \omega^{(0)}(\mathbf{r}) = \frac{\omega^{(2)}(\mathbf{r})}{4\pi R^2}, \qquad \boldsymbol{\omega}^{(1)}(\mathbf{r}) = \frac{\boldsymbol{\omega}^{(2)}(\mathbf{r})}{4\pi R} \tag{6.4.8}$$

The vector functions are needed to account for the discontinuity in the step function. Then

$$\Theta\big(|\mathbf{r}| - 2R\big) = 2\big(\omega^{(3)} \otimes \omega^{(0)} + \omega^{(2)} \otimes \omega^{(1)} + \boldsymbol{\omega}^{(2)} \otimes \boldsymbol{\omega}^{(1)}\big) \tag{6.4.9}$$

where the convolution of two vector functions also implies a scalar product; this result is most easily verified by taking Fourier transforms. In the limit $\mathbf{k} \to 0$, the transforms of the scalar characteristic functions are related to the scaled-particle variables by

$$\rho\hat{\omega}^{(\alpha)}(\mathbf{k} = 0) = \xi_\alpha, \quad \alpha = 0 \text{ to } 3 \tag{6.4.10}$$

while the transforms of the vector functions vanish:

$$\hat{\boldsymbol{\omega}}^{(\alpha')}(\mathbf{k} = 0) = 0, \quad \alpha' = 1,\ 2 \tag{6.4.11}$$

Use of the characteristic functions (6.4.5), (6.4.7) and (6.4.8) as a basis therefore allows the PY direct correlation function to be expressed as a linear combination of convolutions in the form

$$c(r) = \sum_\alpha \sum_\beta c_{\alpha\beta}\, \omega^{(\alpha)} \otimes \omega^{(\beta)} \tag{6.4.12}$$

where a simplified notation is adopted in which the sums on α and β run over both scalar and vector functions; the density-dependent coefficients $c_{\alpha\beta}$ are proportional[7] to the functions $\chi^{(\alpha)}$ defined by (6.4.2). A different set of basis functions that does not involve vector functions has been proposed, but this turns out to be equivalent to the one we have described in the sense that it leads ultimately to the same free-energy functional.[10]

The key assumption of fundamental-measure theory is that the excess free-energy functional has the form

$$\beta\mathcal{F}^{\text{ex}}\big[\rho^{(1)}\big] = \int \Phi^{\text{ex}}\big(\{\bar{\rho}_\alpha(\mathbf{r}')\}\big)\, \mathrm{d}\mathbf{r}' \tag{6.4.13}$$

where the free-energy density Φ^{ex} (in units of $k_{\text{B}}T$) is a function of a set of weighted densities, each defined in the manner of (6.2.16), i.e.

$$\bar{\rho}_\alpha(\mathbf{r}) = \int w_\alpha\big(|\mathbf{r}-\mathbf{r}'|\big)\rho^{(1)}(\mathbf{r}')\,\mathrm{d}\mathbf{r}' \tag{6.4.14}$$

It follows from (3.5.2) that if the scheme contained in (6.4.13) and (6.4.14) is adopted, the direct correlation function of the uniform fluid is of the form

$$c(r) = -\sum_\alpha \sum_\beta \frac{\partial^2 \Phi^{\text{ex}}}{\partial\bar{\rho}_\alpha \partial\bar{\rho}_\beta} w_\alpha \otimes w_\beta \tag{6.4.15}$$

Comparison of (6.4.15) with (6.4.12) suggests immediately that the appropriate choice of weight functions in (6.4.14) are the characteristic functions $\omega^{(\alpha)}(\mathbf{r})$ and $\boldsymbol{\omega}^{(\alpha')}(\mathbf{r})$, and hence that the set $\{\bar{\rho}_\alpha\}$ is one consisting of four scalar and two vector densities:

$$\begin{aligned}
\bar{\rho}_\alpha(\mathbf{r}) &= \int \omega^{(\alpha)}\big(|\mathbf{r}-\mathbf{r}'|\big)\rho^{(1)}(\mathbf{r}')\,\mathrm{d}\mathbf{r}', \quad \alpha = 0 \text{ to } 3 \\
\bar{\boldsymbol{\rho}}_{\alpha'}(\mathbf{r}) &= \int \boldsymbol{\omega}^{(\alpha')}(\mathbf{r}-\mathbf{r}')\rho^{(1)}(\mathbf{r}')\,\mathrm{d}\mathbf{r}', \quad \alpha' = 1,\ 2
\end{aligned} \tag{6.4.16}$$

If the system is homogeneous, the scalar weighted densities reduce to the scaled-particle variables (6.4.2) and the vectorial densities vanish. The scalar densities have the dimensions of the corresponding ξ_α, i.e. $[\text{L}]^{\alpha-3}$; $\bar{\boldsymbol{\rho}}_1$ and $\bar{\boldsymbol{\rho}}_2$ have the same dimensions as $\bar{\rho}_1$ and $\bar{\rho}_2$, respectively.

The precise functional form of the free-energy density remains to be specified. One obvious possibility, in the spirit of a virial expansion, is to write Φ^{ex} as a linear combination of the lowest powers of the weighted densities and their products. In that case, since Φ^{ex} is a scalar with the dimensions of density, it can only be a sum of terms in $\bar{\rho}_0$, $\bar{\rho}_1\bar{\rho}_2$, $\bar{\rho}_2^3$, $\bar{\boldsymbol{\rho}}_1 \cdot \bar{\boldsymbol{\rho}}_2$ and $\bar{\rho}_2(\bar{\boldsymbol{\rho}}_2 \cdot \bar{\boldsymbol{\rho}}_2)$, with coefficients that are functions of the dimensionless density $\bar{\rho}_3$. Thus

$$\Phi^{\text{ex}}\big(\{\bar{\rho}_\alpha\}\big) = \phi_0\bar{\rho}_0 + \phi_1\bar{\rho}_1\bar{\rho}_2 + \phi_2\bar{\rho}_2^3 + \phi_3\bar{\boldsymbol{\rho}}_1 \cdot \bar{\boldsymbol{\rho}}_2 + \phi_4\bar{\rho}_2(\bar{\boldsymbol{\rho}}_2 \cdot \bar{\boldsymbol{\rho}}_2) \tag{6.4.17a}$$

or, in the case of a uniform fluid:

$$\Phi^{\text{ex}}\big(\{\xi_\alpha\}\big) = \phi_0\xi_0 + \phi_1\xi_1\xi_2 + \phi_2\xi_2^3 \tag{6.4.17b}$$

The excess free-energy functional follows from (6.4.13) and the corresponding excess grand potential is

$$\Omega^{\text{ex}}\big[\rho^{(1)}\big] \equiv -\int P^{\text{ex}}\big[\rho^{(1)}\big]\,\mathrm{d}\mathbf{r} = \mathcal{F}^{\text{ex}}\big[\rho^{(1)}\big] - \int \rho^{(1)}(\mathbf{r})\frac{\delta\mathcal{F}^{\text{ex}}}{\delta\rho^{(1)}(\mathbf{r})}\,\mathrm{d}\mathbf{r} \tag{6.4.18}$$

Hence the excess-pressure $P^{\rm ex}$ (a functional of $\rho^{(1)}$) is given by the expression

$$\beta P^{\rm ex}\big[\rho^{(1)}\big] = -\Phi^{\rm ex} + \sum_{\alpha} \bar{\rho}_{\alpha}(\mathbf{r}) \frac{\partial \Phi^{\rm ex}}{\partial \bar{\rho}_{\alpha}} \tag{6.4.19}$$

where the sum runs over all densities in the set $\{\bar{\rho}_{\alpha}\}$.

Now consider the problem from the point of view of scaled-particle theory, which provides an approximation for the excess chemical potential $\mu_{\nu}^{\rm ex}$ of a solute particle of radius R_{ν} in a uniform fluid of hard spheres. It is shown in Appendix E that in the limit $R_{\nu} \to \infty$, $\mu_{\nu}^{\rm ex} \to P V_{\nu}$, where V_{ν} is the volume of the particle and P is the bulk pressure. But it follows from (6.4.17b), as applied to a mixture, that the chemical potential of the solute, $\mu_{\nu}^{\rm ex} = k_{\rm B}T(\partial \Phi^{\rm ex}/\partial \rho_{\nu})$, must also satisfy the relation

$$\beta \mu_{\nu}^{\rm ex} = \sum_{\alpha} \frac{\partial \Phi^{\rm ex}}{\partial \xi_{\alpha}} \frac{\partial \xi_{\alpha}}{\partial \rho_{\nu}} = \frac{\partial \Phi^{\rm ex}}{\partial \xi_3} V_{\nu} + \mathcal{O}\big(R_{\nu}^2\big) \tag{6.4.20}$$

Thus the derivative $\partial \Phi^{\rm ex}/\partial \xi_3$ can be identified as βP. Within fundamental-measure theory the further assumption is now made that the analogous relation is valid for the inhomogeneous fluid, i.e. that

$$\frac{\partial \Phi^{\rm ex}}{\partial \bar{\rho}_3} = \beta P^{\rm ex}\big[\rho^{(1)}\big] + \bar{\rho}_0 \tag{6.4.21}$$

and combination of (6.4.19) and (6.4.21) yields a differential equation for the free-energy density in the form

$$-\Phi^{\rm ex} + \sum_{\alpha} \bar{\rho}_{\alpha} \frac{\partial \Phi^{\rm ex}}{\partial \bar{\rho}_{\alpha}} + \bar{\rho}_0 = \frac{\partial \Phi^{\rm ex}}{\partial \bar{\rho}_3} \tag{6.4.22}$$

Substitution of (6.4.17a) into (6.4.22), and identification of the coefficients of the basis functions in the expansion (6.4.17a), then leads to five, first-order differential equations, one for each of the coefficients ϕ_i; these equations are easily solved to give

$$\begin{aligned} &\phi_0 = -\ln(1-\bar{\rho}_3) + c_0, \qquad \phi_1 = \frac{c_1}{1-\bar{\rho}_3} \\ &\phi_2 = \frac{c_2}{(1-\bar{\rho}_3)^2}, \qquad \phi_3 = \frac{c_3}{1-\bar{\rho}_3}, \qquad \phi_4 = \frac{c_4}{(1-\bar{\rho}_3)^2} \end{aligned} \tag{6.4.23}$$

The constants of integration, c_i, are chosen to ensure that both the free energy and its second functional derivative, i.e. the two-particle direct correlation function (see (3.5.2)), go over correctly to their known, low-density limits in the case of a uniform fluid.[11] These constraints give $c_0 = 0$, $c_1 = 1$, $c_2 = 1/24\pi$, $c_3 = -1$ and $c_4 = -1/8\pi$.[12] The excess free-energy density is thereby completely determined and may be written in the form

$$\Phi^{\rm ex}\big(\{\bar{\rho}_{\alpha}\}\big) = \Phi_1 + \Phi_2 + \Phi_3 \tag{6.4.24}$$

with

$$\Phi_1 = -\bar{\rho}_0 \ln(1-\bar{\rho}_3), \qquad \Phi_2 = \frac{\bar{\rho}_1\bar{\rho}_2 - \bar{\boldsymbol{\rho}}_1 \cdot \bar{\boldsymbol{\rho}}_2}{1-\bar{\rho}_3}$$
$$\Phi_3 = \frac{\bar{\rho}_2^3 - 3\bar{\rho}_2(\bar{\boldsymbol{\rho}}_2 \cdot \bar{\boldsymbol{\rho}}_2)}{24\pi(1-\bar{\rho}_3)^2} \tag{6.4.25}$$

which reduces to the scaled-particle result (6.4.4) for a uniform fluid. The two-particle direct correlation function obtained by differentiation of the free energy reduces in turn to the PY expression (6.4.1), while the third functional derivative yields a three-particle function in good agreement with the results of Monte Carlo calculations.[13] As Figure 4.2 shows, the scaled-particle (or PY compressibility) equation of state slightly overestimates the pressure of the hard-sphere fluid. Some improvement in performance can therefore be expected if the assumed form of the free-energy density is modified in such a way as to recover the Carnahan–Starling equation of state (3.9.17) in the uniform-fluid limit.[14]

The theory is easily generalised to the case of hard-sphere mixtures. Scalar and vectorial characteristic functions $\omega_\nu^{(\alpha)}(\mathbf{r})$ and $\boldsymbol{\omega}_\nu^{(\alpha)}$ are defined for each species ν in a manner completely analogous to the one-component case, with R_ν replacing R. The characteristic functions are then used as weight functions in the definition of a set of global weighted densities:

$$\bar{\rho}_\alpha(\mathbf{r}) = \sum_\nu \int \omega_\nu^{(\alpha)}\big(|\mathbf{r}-\mathbf{r}'|\big)\rho_\nu^{(1)}(\mathbf{r}')\,\mathrm{d}\mathbf{r}', \quad \alpha = 0 \text{ to } 3$$
$$\bar{\boldsymbol{\rho}}_{\alpha'}(\mathbf{r}) = \sum_\nu \int \boldsymbol{\omega}_\nu^{(\alpha')}\big(|\mathbf{r}-\mathbf{r}'|\big)\rho_\nu^{(1)}(\mathbf{r}')\,\mathrm{d}\mathbf{r}', \quad \alpha' = 1,\ 2 \tag{6.4.26}$$

where $\rho_\nu^{(1)}$ is the density profile of species ν, and the free-energy density of the mixture is again given by (6.4.25), or some other, improved form.

The same general approach[15] can be used to derive free-energy functionals for hard-core systems in dimensions $\mathcal{D} = 1$ (hard rods) or $\mathcal{D} = 2$ (hard disks). For $\mathcal{D} = 1$, where only two weight functions are required, this leads to the exact hard-rod functional due to Percus.[16] For $\mathcal{D} = 2$, the procedure is less straightforward, since the decomposition of the Mayer function analogous to (6.4.9) is not achievable with any finite set of basis functions and the PY equation does not have an analytical solution. One and two-dimensional hard-core systems may be regarded as special cases of a hard-sphere fluid confined to a cylindrical pore ($\mathcal{D} = 1$) or a narrow slit ($\mathcal{D} = 2$) for which the diameter of the cylinder or width of the slit is equal to the hard-sphere diameter. Narrow confinement therefore corresponds to a reduction in effective dimensionality or "dimensional crossover", the most extreme example of which ($\mathcal{D} = 0$) occurs when a hard sphere is confined to a spherical cavity large enough to accommodate at most one particle. If the $\mathcal{D} = 3$ functional is to be used in studies of highly confined fluids, it is clearly desirable that it should reduce to the appropriate one- or two-dimensional functional for density profiles of the form $\rho^{(1)}(\mathbf{r}) = \rho^{(1)}(x)\delta(y)\delta(z)$ (for $\mathcal{D} = 1$) or $\rho^{(1)}(\mathbf{r}) = \rho^{(1)}(x, y)\delta(z)$ (for $\mathcal{D} = 2$). This turns out not to be the case. The

exact results for $\mathcal{D}=0$ and $\mathcal{D}=1$ are recovered if the term Φ_3 in (6.4.25) is omitted, but this leads to a considerable deterioration in the results for $\mathcal{D}=3$. A good compromise is achieved[17] if Φ_3 is replaced by

$$\Phi_3' = \frac{\bar{\rho}_2^3}{24\pi(1-\bar{\rho}_3)^2}\left(1-\xi^2\right)^3 \tag{6.4.27}$$

where $\xi(\mathbf{r}) = |\bar{\boldsymbol{\rho}}_2(\mathbf{r})/\bar{\rho}_2(\mathbf{r})|$. The modified term vanishes for $\mathcal{D}=0$ and is numerically small, except at the highest densities, for $\mathcal{D}=1$. In addition, since Φ_3' differs from Φ_3 only by terms of order ξ^4, differentiation of the resulting functional still leads to the PY result for the direct correlation function of the uniform fluid. However, the modification is essentially empirical in nature. A more systematic method of constructing free-energy functionals with the correct dimensional-crossover properties is to start from the exact result for $\mathcal{D}=0$ and build in successively the additional terms needed in higher dimensions.[18] That the functional should have at least the correct qualitative behaviour for $\mathcal{D}=0$ is essential for application to the solid phase, where each particle is confined to the nearly spherical cage formed by its nearest neighbours. The contribution from Φ_3 diverges to negative infinity in the zero-dimensional limit. Thus the theory in its unmodified form cannot account for solid–fluid coexistence, since the solid is always the stable phase.

6.5 CONFINED FLUIDS

The density-functional formalism has been successfully applied to a wide range of physical problems involving inhomogeneous fluids. In this section we describe some of the results obtained from calculations for fluids in confined geometries. The simplest example, illustrated in Figure 6.3, is that of a fluid near a hard, planar wall that confines the fluid strictly to a half-space $z \geqslant 0$, say, where the normal to the wall is taken as the z-axis. The particles of the fluid interact with the wall via a potential $\phi(z)$, which plays the role of the external potential in the theoretical treatment developed in earlier sections. For a hard wall the potential has a purely excluded-volume form, i.e. $\phi(z)=\infty,\ z<0,\ \phi(z)=0,\ z>0$, but more generally it will contain a steeply repulsive term together with a longer ranged, attractive part. If the particles making up the wall are assumed to interact with those of the fluid through a Lennard-Jones potential with parameters ε and σ, integration over a continuous distribution of particles within the wall leads to a wall–fluid potential given by

$$\phi(z) = \tfrac{2}{3}\pi\rho_{\mathrm{W}}\sigma^3\varepsilon\left[\tfrac{2}{15}(\sigma/z)^9 - (\sigma/z)^3\right] \tag{6.5.1}$$

where ρ_{W} is the density of particles in the wall; the surface of the wall is now at $z=0$. This so-called 9-3 potential has been widely adopted as a model of the wall–fluid interaction.

The density profile of a fluid against a planar wall is a function of the single coordinate z. If the bulk density ρ_{B} (the density far from the wall) is sufficiently large, the profile has a pronounced layer structure that extends several particle diameters into the fluid. When all interactions are of hard-core type, $\rho^{(1)}(z)$ may be calculated by density-functional theory

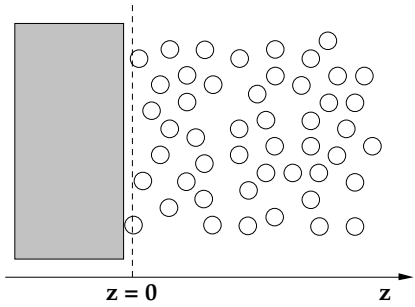

FIG. 6.3. A fluid confined by a hard wall; the centres of interaction of the particles are restricted to the region $z > 0$. For hard spheres of diameter d, the surface of the wall is at $z = -\frac{1}{2}d$.

with the boundary conditions:

$$\lim_{z\to\infty} \rho^{(1)}(z) = \rho_{\mathrm{B}} \tag{6.5.2a}$$

$$\lim_{z\to 0+} \rho^{(1)}(z) = \beta P \tag{6.5.2b}$$

where P is the bulk pressure; these conditions must be supplemented by the requirement that $\rho^{(1)}(z) = 0$ for $z < 0$. Equation (6.5.2b) is an expression of the *contact theorem*, $z = 0$ being the distance of closest approach of a hard sphere of diameter d to a hard wall with a surface at $z = -\frac{1}{2}d$ (see Figure 6.3). The proof of the contact theorem is similar to that of the relation (2.5.26) between the pressure of a uniform hard-sphere fluid and the value of the pair distribution function at contact. The density profile of a fluid against a hard wall is discontinuous at $z = 0$, but whatever the nature of the wall–fluid interaction the density profile can always be written in the form $\rho^{(1)}(z) = \exp[-\beta\phi(z)]y(z)$, where $y(z)$ is a continuous function of z, analogous to the cavity distribution function of a homogeneous fluid. The pressure exerted by the fluid on the wall must be balanced by the force per unit area exerted by the wall on the fluid, i.e.

$$P = -\int_0^\infty \frac{\mathrm{d}\phi(z)}{\mathrm{d}z}\rho^{(1)}(z)\,\mathrm{d}z = k_{\mathrm{B}}T\int_0^\infty \frac{\mathrm{d}}{\mathrm{d}z}\exp\bigl[-\beta\phi(z)\bigr]y(z)\,\mathrm{d}z \tag{6.5.3a}$$

and hence, in the case of a hard wall:

$$P = k_{\mathrm{B}}T\int_0^\infty \delta(z)y(z)\,\mathrm{d}z = k_{\mathrm{B}}T\rho^{(1)}(z = 0+) \tag{6.5.3b}$$

which is (6.5.2b).

The layering of a high-density, hard-sphere fluid near a hard wall is illustrated in Figure 6.4, where comparison is made between the density profile derived from fundamental-measure theory and results obtained by Monte Carlo calculations. Agreement between theory and simulation is excellent. The only significant discrepancies (not visible in the figure)

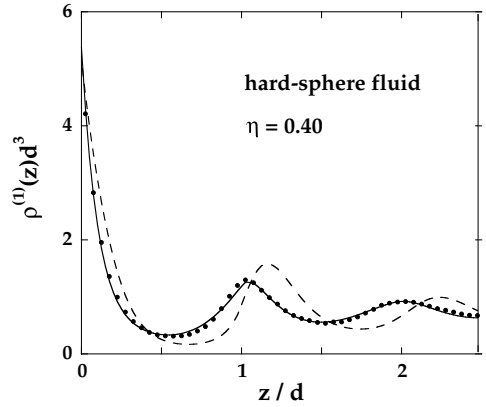

FIG. 6.4. Density profile of a hard-sphere fluid close to a hard wall at a packing fraction $\eta = 0.40$. The full curve is calculated from fundamental-measure theory and the points show the results of Monte Carlo calculations.[19] The dashed curve is calculated from the simpler weighted-density approximation provided by (6.2.22).

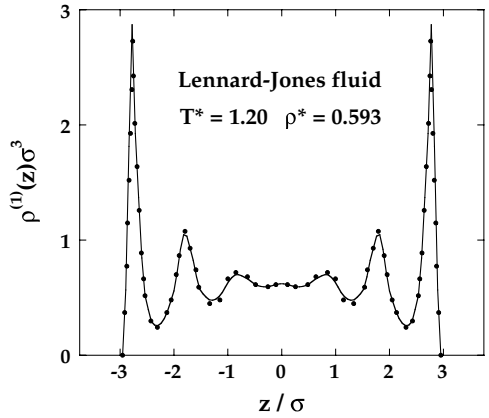

FIG. 6.5. Density profile of a Lennard-Jones fluid in a slit of width $L = 7.5\sigma$. The curve is calculated from fundamental-measure theory and the points show the results of a Monte Carlo simulation.[20] After Kierlik and Rosinberg.[21]

occur close to contact, where the theoretical values are too high. The source of these small errors lies in the fact that in the theory as implemented here the value at contact is determined, via the boundary condition (6.5.2b), by the pressure calculated from scaled-particle theory. As discussed in Section 6.4, such errors can be largely eliminated if the free-energy functional is tailored to reproduce a more accurate equation of state.

Though designed for systems of hard particles, fundamental-measure theory can also be used to calculate the density profiles and associated thermodynamic properties of a wider class of fluids if combined with the methods of perturbation theory described in Chapter 5. We suppose, as usual, that the pair potential $v(r)$ of the system of interest can be divided

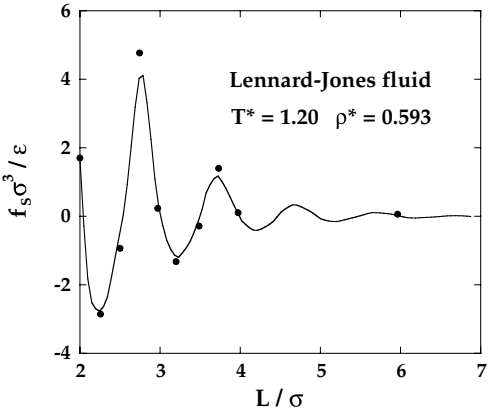

FIG. 6.6. Solvation force for a Lennard-Jones fluid in a slit as a function of slit width L. The curve is calculated from fundamental-measure theory and the points show the results of a Monte Carlo simulation.[22] After Kierlik and Rosinberg.[21]

into a reference part, $v_0(r)$, and a perturbation, $w(r)$. Then (3.4.10) provides an exact relation between the free-energy functional corresponding to the full potential, $\mathcal{F}[\rho^{(1)}]$, and that of the reference system, $\mathcal{F}_0[\rho^{(1)}]$. The obvious choice of reference system is again a fluid of hard spheres of diameter d given, say, by the Barker–Henderson prescription (5.3.11). If the perturbation is sufficiently weak to be treated in a mean-field approximation, the correlation term in (3.4.10) can be ignored. The grand-potential functional to be minimised is then of the form

$$\Omega_\phi[n] = \mathcal{F}_d[n] + \tfrac{1}{2}\iint n(\mathbf{r})w(\mathbf{r},\mathbf{r}')n(\mathbf{r}')\,\mathrm{d}\mathbf{r}\,\mathrm{d}\mathbf{r}' + \int n(\mathbf{r})\big[\phi(\mathbf{r}) - \mu\big]\,\mathrm{d}\mathbf{r} \qquad (6.5.4)$$

where $\mathcal{F}_d[\rho^{(1)}]$ is the free-energy functional of the hard-sphere system, taken to be of fundamental-measure form, and $n(\mathbf{r})$ is a trial density. This approximation has been widely used in a variety of applications to confined fluids. An example of the results obtained for the density profile of a Lennard-Jones fluid confined to a slit formed by two parallel plates separated by a distance L is pictured in Figure 6.5; the wall–fluid potential has a form similar to (6.5.1). When $L/\sigma \approx 3$, the density profile has a double-peaked structure, with maxima close to the walls of the slit. As the slit width increases, the number of layers of particles that can be accommodated also increases, with a third peak appearing initially mid-way between the walls. In the example shown, corresponding to $L/\sigma = 7.5$, six clearly defined layers can be detected, together with a weak maximum at the centre of the slit. The agreement with simulations is again outstandingly good. Figure 6.6 shows the solvation force as a function of L for the same system, calculated from the microscopic expression

$$f_S = -\int_0^L \frac{\mathrm{d}\phi(z)}{\mathrm{d}z}\rho^{(1)}(z)\,\mathrm{d}z - P \qquad (6.5.5)$$

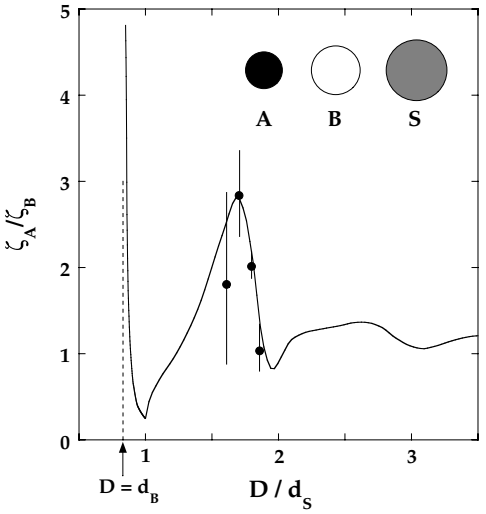

FIG. 6.7. Selective absorption by a cylindrical pore of solute hard-spheres (A, B) at low concentration in a solvent of larger spheres (S) as a function of the cylinder diameter. The curve is calculated from fundamental-measure theory and the points with error bars show the results of Monte Carlo calculations. See text for details. After Goulding *et al*.[24]

which is easily derived from the definition (6.1.15). The force is seen to oscillate around zero, its asymptotic value as $L \to \infty$. Oscillatory solvation forces are a direct consequence of the layering evident in Figure 6.5; they have been observed experimentally with the aid of "surface-force machines", which have a spatial resolution better than 1 Å. The amplitude of oscillation decreases rapidly with L, and is already negligible for $L = 7.5\sigma$ despite the high degree of layering still observed at this separation.

Functionals of the general form represented by (6.5.4), with various levels of approximation for the reference-system contribution, have also been used extensively in studies of phenomena such as capillary condensation in a narrow pore and the wetting of solid substrates.[23] The two effects are closely related and each is strongly dependent on the nature of the interaction between the fluid and the confining surface. Capillary condensation is the phenomenon whereby a confined gas condenses to a liquid at a chemical potential below that corresponding to liquid–vapour coexistence in the bulk. Wetting is an interfacial phase transition for which the adsorption defined by (6.1.13) (with $L \to \infty$) acts as an order parameter by providing a measure of the thickness of the liquid film adsorbed on the substrate. As the temperature increases along the liquid–vapour coexistence line, the film thickness, which is of microscopic dimensions at low temperatures, diverges either continuously (corresponding to a second-order wetting transition) or discontinuously (a first-order transition) as the wetting temperature T_w, with $T_t < T_w < T_c$, is reached (T_t and T_c being the triple-point and critical temperatures, respectively).

A different type of problem to which density-functional theory has been successfully applied concerns the size selectivity of porous materials in which the pores have a confining length of molecular dimensions. As a simple example, consider an infinitely long,

cylindrical pore of diameter D connecting two reservoirs that contain a three-component mixture of hard spheres under identical physical conditions (packing fraction and concentrations). The fluid in the reservoirs consists of a majority component – the "solvent" S – at a packing fraction $\eta = 0.41$, and two "solute" components, A and B, at concentrations of 0.05 M, with relative hard-sphere diameters $d_A : d_B : d_S$ appropriate to water (S) and the ions Na^+ (A) and K^+ (B).[24] Spheres of different diameters will permeate the pore to different extents, and at equilibrium the chemical potentials of each species will be the same inside the pore as in the reservoirs. The density profiles within the pore depend only on the radial distance r from axis of the cylinder; they can be calculated by minimising a fundamental-measure functional, modified in the manner represented by (6.4.27) to cater for the quasi-one-dimensional nature of the confinement. The degree of permeation (or "absorbance") ζ_ν of species ν may be defined as the ratio of the mean density of particles of that species inside the pore to the density of the same species in the reservoirs. When the cylinder diameter D is comparable with the sphere diameters, the pore absorbs preferentially one of the two solutes. The selectivity of the pore is measured by the relative absorbance ζ_A/ζ_B, plotted as a function of cylinder diameter in Figure 6.7. This varies with D by a factor of order 10, in fair agreement with calculations by a grand-canonical Monte Carlo method, though the low concentrations of solute particle mean that the statistical uncertainties in the results of the simulations are large. When $d_B < d_S$, only A-particles can be absorbed. Thus, for cylinder diameters only slightly larger than d_B, the selectivity is initially very large but falls rapidly as D increases. When $D \approx d_S$, the larger solute is up to four times more likely to be adsorbed than the smaller one, a purely entropic effect that is somewhat counterintuitive. However, when the cylinder diameter exceeds d_S and solvent particles can enter the pore, the selectivity rises, reaching a maximum value of about 2.8 at $D \approx 1.7 d_S$. The degree of selectivity can be greatly enhanced by changes in the relative diameters of the species involved.

6.6 DENSITY-FUNCTIONAL THEORY OF FREEZING

If cooled or compressed sufficiently gently, a liquid will freeze into an ordered, solid phase. The transition is accompanied by a discontinuous change in volume, $\Delta V = V_L - V_S$, which is usually positive (water is a notable exception), and by a latent heat, $T\Delta S$, which is always positive. The discontinuities in V and S, both of which are first derivatives of the free energy, are the signatures of a first-order phase transition. Freezing of simple liquids is largely driven by entropic factors, a fact most obvious in the case of the hard-sphere fluid, since the nature of the hard-sphere interaction means that the difference in free energy of the solid and fluid phases at a given temperature is equal to $-T\Delta S$. One of the most significant findings to emerge from the earliest molecular simulations[25] was that the hard-sphere fluid freezes into a stable, face-centred cubic crystal; accurate calculations[26] of the free energies of the fluid and solid as functions of density subsequently showed that the packing fractions at coexistence are $\eta_F \approx 0.494$ and $\eta_S \approx 0.545$. We can obtain a rough estimate of the configurational entropy in the two phases by temporarily ignoring the correlations between particles brought about by excluded-volume effects. If we treat the fluid

as a system of non-interacting particles moving freely in a volume V and the solid as a system of localised (and hence distinguishable) particles in which each particle is confined by its neighbours to a region of order V/N around its lattice site, a simple calculation shows that the configurational entropy per particle of the solid lies below that of the fluid by an amount equal to k_B. In reality, of course, correlations make a large contribution to the entropy, which at densities beyond $\eta \approx 0.5$ must be appreciably larger for the "ordered" solid than for the "disordered" fluid, since the solid is the stable phase. The explanation of this apparent paradox is the fact that the free volume available to a particle is larger in the solid than in the "jammed" configurations that are generated when a fluid is over-compressed. This ties in with Bernal's observation that the maximum density achievable by random packing of hard spheres ($\eta \approx 0.65$) lies well below that of the face-centred cubic structure ($\eta \approx 0.74$).

The relative volume change on freezing of a hard-sphere fluid is $|\Delta V|/V \approx 0.10$ and the entropy change per particle is $\Delta S/Nk_B \approx 1.16$. Simple perturbation theory shows that the effect of adding an attractive term to the hard-sphere interaction is to broaden the freezing transition, i.e. to increase the relative volume change, but the opposite effect occurs if the short-range repulsion is softened. In the case of the soft-sphere potentials defined by (5.2.25), for example, the relative volume change is found to decrease rapidly[27] with reduction in the exponent n, becoming strictly zero[28] in the limiting case of the one-component plasma ($n = 1$). The change in entropy also decreases with n, but much more slowly, and remains close to k_B per particle. Both experiments and simulations show that for a wide variety of systems consisting of spherical or nearly spherical particles the amplitude of the main peak in the static structure factor at freezing is approximately 2.85. This provides a useful criterion for freezing that appears to be independent of the crystal structure of the solid phase.[29] It applies, for example, to the family of soft-sphere fluids, for which the stable crystal phase is face-centred cubic at large values of n but body-centred cubic for softer potentials.

The lattice structure of a crystalline solid means that the density profile must be a periodic function of $\mathbf{r}$ such that

$$\rho^{(1)}(\mathbf{r} + \mathbf{R}_i) = \rho^{(1)}(\mathbf{r}) \tag{6.6.1}$$

where the set $\{\mathbf{R}_i\}$ represents the lattice coordinates of the particles in the perfectly ordered crystal. Let $\mathbf{u}_i = \mathbf{r}_i - \mathbf{R}_i$ be the displacement of particle i from its equilibrium position. Then the Fourier transform of the density profile can be written (see (3.1.4)) as

$$\hat{\rho}^{(1)}(\mathbf{k}) = \sum_{i=1}^{N} \langle \exp(-i\mathbf{k}\cdot\mathbf{r}_i) \rangle = \sum_{i=1}^{N} \exp(-i\mathbf{k}\cdot\mathbf{R}_i) \langle \exp(-i\mathbf{k}\cdot\mathbf{u}_i) \rangle \tag{6.6.2}$$

Away from any interface, all lattice sites are equivalent, and the second statistical average in (6.6.2) is therefore independent of i. Thus

$$\hat{\rho}^{(1)}(\mathbf{k}) = \langle \exp(-i\mathbf{k}\cdot\mathbf{u}) \rangle \sum_{i=1}^{N} \exp(-i\mathbf{k}\cdot\mathbf{R}_i) \tag{6.6.3}$$

The sum over lattice sites is non-zero only if $\mathbf{k}$ coincides with a reciprocal lattice vector $\mathbf{G}$. Hence

$$\sum_{i=1}^{N} \exp(-i\mathbf{k}\cdot\mathbf{R}_i) = N\delta_{\mathbf{k},\mathbf{G}} \tag{6.6.4}$$

and the only non-zero Fourier components of the density are

$$\hat{\rho}^{(1)}(\mathbf{G}) = N\big\langle \exp(-i\mathbf{G}\cdot\mathbf{u})\big\rangle \tag{6.6.5}$$

In the harmonic-phonon approximation, valid for small-amplitude vibrations of the particles around their lattice positions, the displacement vectors $\mathbf{u}$ have a gaussian distribution:

$$\big\langle \exp(-i\mathbf{G}\cdot\mathbf{u})\big\rangle = \exp\big(-\tfrac{1}{6}G^2\langle u^2\rangle\big) \tag{6.6.6}$$

where $\langle u^2\rangle$ is the mean-square displacement of a particle from its lattice site. If we substitute (6.6.6) in (6.6.5) and take the inverse transform, we find that

$$\begin{aligned}
\rho^{(1)}(\mathbf{r}) &= \frac{1}{V}\sum_{\mathbf{G}}\sum_{i=1}^{N} \exp\big(i\mathbf{G}\cdot(\mathbf{r}-\mathbf{R}_i)\big)\exp\big(-\tfrac{1}{6}G^2\langle u^2\rangle\big) \\
&\approx \frac{1}{(2\pi)^3}\sum_{i=1}^{N}\int \exp\big(i\mathbf{G}\cdot(\mathbf{r}-\mathbf{R}_i)\big)\exp\big(-\tfrac{1}{6}G^2\langle u^2\rangle\big)\,\mathrm{d}\mathbf{G} \\
&= \left(\frac{\alpha}{\pi}\right)^{3/2}\sum_{i=1}^{N}\exp\big(-\alpha(\mathbf{r}-\mathbf{R}_i)^2\big)
\end{aligned} \tag{6.6.7}$$

where $\alpha = (3/2\langle u^2\rangle)$ is an inverse-width parameter. The density profile of the crystal therefore appears as the sum of N gaussian peaks, each centred on a lattice site $\mathbf{R}_i$. As α increases, the particles become more strongly localised and the peaks become narrower. The most general representation of $\rho^{(1)}(\mathbf{r})$ compatible with lattice periodicity is

$$\rho^{(1)}(\mathbf{r}) = \rho_{\mathrm{S}}\left(1 + \sum_{\mathbf{G}\neq 0}\zeta(\mathbf{G})\exp(i\mathbf{G}\cdot\mathbf{r})\right) \tag{6.6.8}$$

where ρ_{S} is the overall number density of the solid. In the harmonic approximation the coefficients of the "density waves" $\exp(i\mathbf{G}\cdot\mathbf{r})$ are related to the parameter α by

$$\zeta(\mathbf{G}) = \exp\big(-G^2/4\alpha\big) \tag{6.6.9}$$

The vibrational mean-square displacement $\langle u^2\rangle$ can be determined by analysis of the lineshape of the Bragg peaks observed in x-ray or neutron-scattering experiments; it is found to decrease sharply as the crystal is cooled along an isochore or compressed along an isotherm. The quantity $L = \langle u^2\rangle^{1/2}/R_0$, where R_0 is the nearest-neighbour distance in

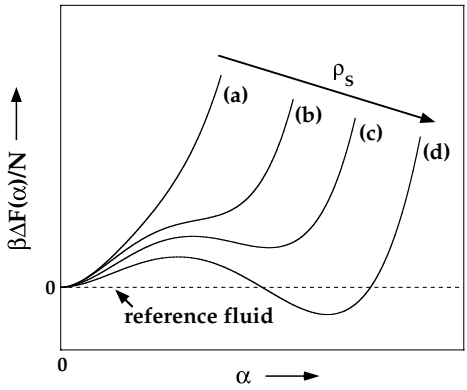

FIG. 6.8. Typical behaviour of the free-energy difference defined by (6.6.11) as a function of the variational parameter α for increasing values of the density ρ_S. Curve (d) corresponds to a density at which the ordered crystal is the stable phase. See text for details.

the crystal, is called the Lindemann ratio. According to the "Lindemann rule", melting should occur when L reaches a value that is only weakly material-dependent and equal to about 0.15. Simulations have shown that for hard spheres the value at melting is approximately 0.13, but is slightly larger for softer potentials. That such a criterion exists is not surprising: instability of the solid can be expected once the vibrational amplitude of the particles becomes a significant fraction of the spacing between neighbouring lattice sites.

The idea that underpins much of the density-functional approach to freezing goes back to the work of Kirkwood and Monroe.[30] While the periodic density profile is clearly very different from the uniform density of the fluid, it is reasonable to assume that the short-range pair correlations in the solid are similar to those of some effective, reference fluid. In other words, a crystal may be regarded as a highly inhomogeneous fluid, and different versions of the theory differ mostly in the choice made for the density of the reference fluid.[31]

We showed in Section 4.3 that expansion of the free-energy functional in powers of $\delta\rho^{(1)}(\mathbf{r})$ around that of a homogeneous fluid of density ρ_0 leads, when truncated at second order, to the expression for the density profile given by (4.3.16). In the application to freezing, there is no external field, and (4.3.16) becomes

$$\rho^{(1)}(\mathbf{r}) = \rho_0 \exp\left(\int c_0^{(2)}(\mathbf{r}-\mathbf{r}')\left[\rho^{(1)}(\mathbf{r}) - \rho_0\right] \mathrm{d}\mathbf{r}' \right) \tag{6.6.10}$$

Higher-order terms in the expansion are easily derived, but explicit calculations become increasingly involved and are therefore rarely attempted. Equation (6.6.10) always has the trivial solution $\rho^{(1)}(\mathbf{r}) = \rho_0$, but at sufficiently high densities there exist, in addition, periodic solutions of the form (6.6.8). In order to decide whether the uniform or periodic solution corresponds to the stable phase, it is necessary to compute the free energies of the two phases. The free energy of the solid phase is related to that of the reference fluid by (4.3.12), where the choice of ρ_0 remains open. It is clear, however, that ρ_0 should be

comparable with ρ_S, the mean number density in the solid, since the density change on freezing is typically less than 10%. One obvious possibility is to set $\rho_0 = \rho_S$, which simplifies the problem because the linear term in (4.3.12) then vanishes, but other choices have been made.[32] If we substitute (6.6.8) (with $\rho_0 = \rho_S$) into the quadratic term in (4.3.12) and use the convolution theorem, we find that

$$\begin{aligned}\frac{\beta \Delta F}{N} &\equiv \frac{\beta \mathcal{F}[\rho^{(1)}]}{N} - \frac{\beta F_0(\rho_S)}{N} \\ &= \int \rho^{(1)}(\mathbf{r}) \ln\left(\frac{\rho^{(1)}(\mathbf{r})}{\rho_S}\right) d\mathbf{r} - \tfrac{1}{2}\rho_S \sum_{\mathbf{G}\neq 0} \hat{c}_0^{(2)}(\mathbf{G}) |\zeta \mathbf{G}|^2 \end{aligned} \tag{6.6.11}$$

The free-energy difference ΔF must now be minimised with respect to $\rho^{(1)}(\mathbf{r})$, i.e. with respect to the order parameters $\zeta_{\mathbf{G}}$. In practice, most calculations are carried out using the gaussian form (6.6.9), in which case the inverse width α is the only variational parameter. The ideal contribution to the free energy favours the homogeneous phase; the quadratic, excess term favours the ordered phase provided the quantities $\hat{c}_0^{(2)}(\mathbf{G})$ are positive for the smallest reciprocal-lattice vectors, since the contributions thereafter decrease rapidly with increasing G. The competition between ideal and excess contributions leads to curves of ΔF versus α of the Landau type, shown schematically in Figure 6.8. When the density ρ_S is low (curves (a) and (b)), there is a single minimum at $\alpha = 0$, corresponding to a homogeneous, fluid phase. At higher densities (curve (c)), a minimum appears at a positive value of ΔF, signalling the appearance of a metastable, crystalline phase. Further increase in density leads to a lowering of the value of ΔF at the second minimum, which eventually becomes negative (curve (d)); the ordered crystal is now the stable phase. Once the free energies of fluid and solid along a given isotherm are known, the densities of the coexisting phases can be determined from the Maxwell double-tangent construction, which ensures equality of the chemical potentials and pressures of the two phases.[8] The calculations are carried out for a given Bravais lattice and hence for a given set of reciprocal-lattice vectors. If the relative stability of different crystal structures is to be assessed, separate calculations are needed for each lattice.

The method we have outlined is essentially that advanced by Ramakrishnan and Yussouff,[33] reformulated in the language of density-functional theory.[34] It works satisfactorily in the case of hard spheres, but the quality of the results deteriorates for softer potentials, for which the stable solid has a body-centred cubic structure. In that case, if the potential is sufficiently soft, the contribution to the sum over $\mathbf{G}$ in (6.6.11) from the second shell of reciprocal-lattice vectors is negative. The resulting contribution to ΔF is therefore positive and sufficiently large to destabilise the solid. This defect in the method can be overcome by inclusion of the third-order term in the expansion of the free-energy functional, but that requires some approximation to be made for the three-particle direct correlation function of the reference system.[35] Other approaches to the problem of freezing have also been used. The most successful of these are variants of fundamental-measure theory of the type discussed at the end of Section 6.4, which lead to values for the densities at coexistence of the hard-sphere fluid and solid that agree with those obtained by simulation to within one percent.

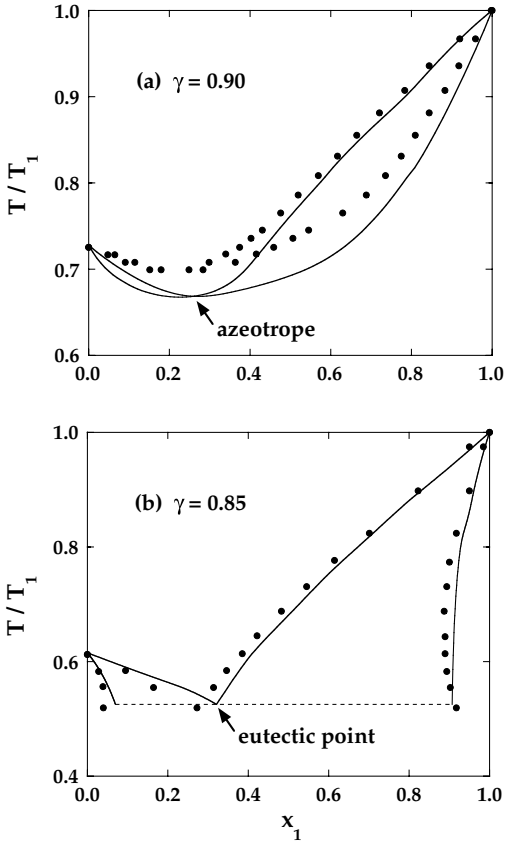

FIG. 6.9. Phase diagrams of binary hard-sphere mixtures at a fixed pressure for two values of the diameter ratio γ; x_1 and T_1 are, respectively, the number concentration of the larger spheres and the freezing temperature for $x_1 = 1$. (a) An azeotropic-type diagram; (b) a eutectic-type diagram. The full curves are calculated from density-functional theory and the points are the results of Monte Carlo calculations;[37] the broken line in (b) shows the miscibility gap at the eutectic temperature. After Zeng and Oxtoby.[36]

The theory can be extended to mixtures and in that form has been used to study the freezing of binary hard-sphere mixtures into substutionally disordered, face-centred-cubic structures, where the nature of the resulting phase diagram depends critically on the value of the diameter ratio, $\gamma = d_1/d_2$. Figure 6.9 shows phase diagrams in the temperature–concentration plane calculated from a version of density-functional theory[36] in which the free-energy of the solid is calculated from a generalisation of the weighted-density approximation (6.2.24); earlier calculations based on a generalisation of (6.6.11) had led to qualitatively similar results.[38] When γ is greater than approximately 0.94, the two species are miscible in all proportions in both phases, the concentration of large spheres being slightly higher in the solid. At lower values of γ ($0.88 < \gamma < 0.93$), the phase diagram has the form shown in part (a) of the figure, in which we see the appearance of an azeotrope, i.e. a point where the coexistence curves pass through a minimum and solid and fluid have identical

compositions. When γ is reduced below 0.88, as in part (b), the azeotrope is replaced by a eutectic point. There is now a wide range of concentration over which the two species are immiscible in the solid; the solubilities of large spheres in a solid consisting mostly of small spheres or vice versa are each less than 10% and become rapidly smaller as γ is further reduced. This behaviour is broadly consistent with the empirical Hume–Rothery rule, according to which the disordered solid phases of metallic alloys become unstable for diameter ratios less than about 0.85. As the figure shows, there is good agreement with the results of simulations both here and in the azeotropic case. Other density-functional calculations[39] have shown that ordered phases of AB_n-type structure remain stable at values of γ below 0.8, which is consistent both with simulations of hard-sphere mixtures and with experimental studies of colloidal suspensions.[40]

NOTES AND REFERENCES

1. For a more detailed treatment of the material discussed in this section, see Evans, R., *In* "Liquids at Interfaces: Les Houches, Session XLVIII" (J. Charvolin, J.F. Joanny and J. Zinn-Justin, eds). Elsevier, Amsterdam, 1990.
2. Biben, T., Hansen, J.P. and Barrat, J.L., *J. Chem. Phys.* **98**, 7330 (1993).
3. It also played a central role in early theoretical work on the wetting transition. See Cahn, J.W., *J. Chem. Phys.* **66**, 3667 (1977).
4. For a critical survey of different approximations, see Evans, R., *In* "Fundamentals of Inhomogeneous Fluids" (D. Henderson, ed.). Marcel Dekker, New York, 1991.
5. Tarazona, P. and Evans, R., *Mol. Phys.* **52**, 847 (1984).
6. (a) Tarazona, P., *Phys. Rev. A* **31**, 2672 (1985). (b) Curtin, W.A. and Ashcroft, N.W., *Phys. Rev. A* **32**, 2909 (1985). (c) Denton, A.R. and Ashcroft, N.W., *Phys. Rev. A* **39**, 4701 (1989).
7. (a) Rosenfeld, Y., *Phys. Rev. Lett.* **63**, 980 (1989). (b) Rosenfeld, Y., Levesque, D. and Weis, J.J., *J. Chem. Phys.* **92**, 6818 (1990).
8. See Chapter 5, Section 5.6.
9. Reiss, H., Frisch, H.L. and Lebowitz, J.L., *J. Chem. Phys.* **31**, 369 (1959).
10. (a) Kierlik, E. and Rosinberg, M.L., *Phys. Rev. A* **42**, 3382 (1990). (b) Phan, S., Kierlik, E., Rosinberg, M.L., Bildstein, B. and Kahl, G., *Phys. Rev. E* **48**, 618 (1993).
11. The detailed calculation for a different but related system (parallel hard cubes) is given by Cuesta, J.A. and Martínez-Ratón, Y., *J. Chem. Phys.* **107**, 6379 (1997).
12. Note that in refs. 7 the signs of the coefficients c_3 and c_4 are incorrect.
13. See Figure 1 in ref. 10(a). The correct results are those given by the full curves: for an explanation, see ref. 10(b).
14. Roth, R., Evans, R., Lang, A. and Kahl, G., *J. Phys. Condens. Matter* **14**, 12063 (2002).
15. Rosenfeld, Y., *Phys. Rev. A* **42**, 5978 (1990).
16. Percus, J.K., *J. Stat. Phys.* **15**, 505 (1976).
17. Rosenfeld, Y., Schmidt, M., Löwen, H. and Tarazona, P., *Phys. Rev. E* **55**, 4245 (1997).
18. Tarazona, P. and Rosenfeld, Y., *Phys. Rev. E* **55**, R4873 (1997). See also González, A., White, J.A. and Evans, R., *J. Phys. Condens. Matter* **9**, 2375 (1997).
19. Groot, R.D., Faber, N.M. and van der Eerden, J.P., *Mol. Phys.* **62**, 861 (1987).
20. Snook, I.K. and van Megen, W., *J. Chem. Phys.* **72**, 2907 (1980).
21. Kierlik, E. and Rosinberg, M.L., *Phys. Rev. A* **44**, 5025 (1991).
22. Magda, J.J., Tirell, M. and Davis, H.T., *J. Chem. Phys.* **83**, 1888 (1985).
23. (a) Evans, R., *J. Phys. Condens. Matter* **2**, 8989 (1990). (b) Gelb, L.V., Gubbins, K.E., Radhakrishnan, R. and Sliwinska-Bartkowiak, M., *Rep. Prog. Phys.* **62**, 1573 (1999).
24. Goulding, D., Melchionna, S. and Hansen, J.P., *Phys. Chem. Chem. Phys.* **3**, 1644 (2001).
25. (a) Alder, B.J. and Wainwright, T.E., *J. Chem. Phys.* **27**, 1208 (1957). (b) Wood, W.W. and Jacobson, J.D., *J. Chem. Phys.* **27**, 1207 (1957).

26. Hoover, W.G. and Ree, F.H., *J. Chem. Phys.* **49**, 3609 (1968).
27. (a) Hoover, W.G., Gray, S.G. and Johnson, K.W., *J. Chem. Phys.* **55**, 1128 (1971). (b) Agrawal, R. and Kofke, D.A., *Phys. Rev. Lett.* **74**, 122 (1995).
28. Weeks, J.D., *Phys. Rev. B* **24**, 1530 (1981).
29. (a) Hansen, J.P. and Verlet, L., *Phys. Rev.* **184**, 151 (1969). (b) Hansen, J.P. and Schiff, D., *Mol. Phys.* **25**, 1281 (1973).
30. Kirkwood, J.G. and Monroe, E., *J. Chem. Phys.* **9**, 511 (1941).
31. Fundamental-measure theory is an exception to this rule.
32. Baus, M., *J. Phys. Condens. Matter* **2**, 2111 (1990).
33. Ramakrishnan, T.V. and Yussouff, M., *Phys. Rev. B* **19**, 2775 (1979).
34. Haymet, A.D.J. and Oxtoby, D.W., *J. Chem. Phys.* **74**, 2559 (1981).
35. See, e.g., Barrat, J.L., Hansen, J.P. and Pastore, G., *Mol. Phys.* **63**, 747 (1988).
36. Zeng, X.C. and Oxtoby, D.W., *J. Chem. Phys.* **93**, 4357 (1990). See also Denton, A.R. and Ashcroft, N.W., *Phys. Rev.* **42**, 7312 (1990).
37. Kranendonk, W.G.T. and Frenkel, D., *Mol. Phys.* **72**, 679 (1991).
38. Barrat, J.L., Baus, M. and Hansen, J.P., *J. Phys. C* **20**, 1413 (1987).
39. Xu, H. and Baus, M., *J. Phys. Condens. Matter* **4**, L663 (1992).
40. Bartlett, P., Ottewill, R.H. and Pusey, P.N., *Phys. Rev. Lett.* **68**, 3801 (1992).